

THESIS

This is to certify that the

dissertation entitled

Exact Ground States Of Disordered Systems

presented by

Jan Hermann Meinke

has been accepted towards fulfillment of the requirements for

Ph.D. degree in Physics

·

Date 5/3/02

LIBRARY Michigan State University

PLACE IN RETURN BOX to remove this checkout from your record.

TO AVOID FINES return on or before date due.

MAY BE RECALLED with earlier due date if requested.

DATE DUE	DATE DUE	DATE DUE

6/01 c:/CIRC/DateDue.p65-p.15

EXACT GROUND STATES OF DISORDERED SYSTEMS

By

Jan Hermann Meinke

A DISSERTATION

Submitted to
Michigan State University
in partial fulfillment of the requirements
for the degree of

DOCTOR OF PHILOSOPHY

Department of Physics and Astronomy

2002

Abstract

EXACT GROUND STATES OF DISORDERED SYSTEMS

By

Jan Hermann Meinke

Finding the ground state of disordered systems is in general a hard problem. Mappings of disordered systems to problems from computer science for which efficient, i.e., polynomial algorithms are known allow the numerical study of large systems. I study the ground state of the random-field Ising model both analytically using mean field approximations and numerically in 3D. I find that the behavior for the infinite-range model is nonuniversal in the sense that the critical exponent β can vary continuously. On the Cayley tree, however, the behavior is universal.

I develop a theory for the roughening of the minimum energy fracture surface in polycrystalline materials as a function of the relevant energy parameter $\epsilon = \epsilon_i/\epsilon_g$. ϵ_g is the internal binding energy of the grain and ϵ_i is the adhesion energy. Both local and global effects contribute to the roughening and have to be taken into account. This leads to an ϵ -dependent critical length L_c . For systems with $L > L_c$ and $\epsilon < 1$ the interface is always rough.

Contents

Li	st of '	Fables		Vi
Li	st of l	Figures		vii
1	Disc	order ar	nd Complexity	1
2	Ana	lytic M	ethods and Concepts	10
	2.1	Critica	al exponents and scaling theory	11
		2.1.1	The scaling hypothesis	13
	2.2	Ising r	nodel	17
		2.2.1	Mean field theory	20
		2.2.2	Infinite range model	24
		2.2.3	Cayley tree	25
		2.2.4	Renormalization group and universality	26
	2.3	Landa	u theory	29
	2.4	Percol	ation	32
		2.4.1	Cayley tree	35
		2.4.2	Giant clusters in random graphs	38
3	Path	ıs, Dom	ain Walls, and Spin Clusters in Random Media	40
	3.1	Domai	in walls and random bonds	41

	3.2	Spin cl	lusters and random fields	42
4	Max	cimum I	Flow/Minimum Cut	4 4
	4.1	The ma	aximum flow/minimum cut theorem	44
	4.2	Mappi	ngs to the maximum flow/minimum cut problem	46
		4.2.1	Finding the interface in a random-bond Ising model with fixed	
			boundaries	46
		4.2.2	The mapping of the random-field Ising model to the maximum	
			flow/minimum cut problem	48
	4.3	Algori	thms for solving the maximum flow problem	50
		4.3.1	The augmenting path algorithm	50
		4.3.2	Push-relabel	52
	4.4	Benchi	marks	54
5	Ran	dom-Fi	eld Ising Model	56
	5.1		e-range random-field Ising model	
		5.1.1	Bimodal distribution	
		5.1.2	Gaussian distribution	
		5.1.3	Polynomial distributions	
		5.1.4	Finite temperature	
	5.2		tree	
	5.3		rical ground state calculations of the RFIM	
			6	
6	Inte	rfaces ii	n Disordered Systems	76
	6.1	Models	s and methods	77
	6.2		adhesion limit $\epsilon o 0$	
	6.3	Strong	adhesion limit	84
	6.4	Interme	ediate regime	87

	6.5 Summary	96
7	Outlook	97
A	Taylor Expansion of P_+ for the RFIM on the Cayley Tree	99
Bil	bliography	104
In	dex	110

List of Tables

2.1	The standard set of critical thermal exponents	12
2.2	Scaling relations between the critical exponents	17
5.1	Benchmark results for the random-field Ising model	70

List of Figures

1.1	Computer network	3
1.2	Network graph for computer network in Fig. 1.1	4
1.3	Tunable random distribution	7
1.4	Magnetization for different distributions of random fields	7
2.1	Phase diagram of water	10
2.2	Graphical solution of the magnetization in mean field theory	22
2.3	Cayley tree with z=3	26
2.4	Kadanoff's block spins for an Ising model	27
2.5	Percolation on a square lattice	33
4.1	The minimum cut in a random-bond Ising model	48
4.2	Mapping of a 1D random-field Ising model to the maximum flow problem .	49
4.3	Push-relabel Benchmarks	55
5.1	Tunable random distribution	63
5.2	Magnetization for different distributions of random fields	64
5.3	Maximum execution time vs. L	71
5.4	Maximum standard deviation of the magnetization	72
5.5	Finite size scaling of critical width	73
5.6	Scaling plot for the magnitude of the magnetization for ρ_4 with y=0.5	74

5.7	Scaling plot for the magnitude of the magnetization for ρ_4 with y=-0.5	74
6.1	2D Grain Structure	78
6.2	Grain structures with interface	80
6.3	Scaling in the weak adhesion limit	82
6.4	Fraction of grain boundary bonds of the interface vs. ϵ	85
6.5	Average interface energy vs. ϵ	86
6.6	Average roughness vs. ϵ	87
6.7	Average number of interface bond vs. ϵ	88
6.8	Interface through granular material	89
6.9	Scaling of roughness	94

Chapter 1

Disorder and Complexity

The white elephant of the king moved gracefully through the jungle. He briefly paused to take a drink of water from the pond near Ibn Assam's village and then moved on with steady step.

A few days later the elephant was stricken with a terrible illness. None of the king's learned medics could find a cure. Ibn Assam, a poor farmer, offered his services to the king. The king was so desperate that he accepted and promised to grant him a wish if he healed his elephant. Ibn Assam had seen the king's elephant drink from the poisonous pond and had brought some of the herbs he used to heal his goats. After a week's time the animal was on his way to recovery and the king asked Ibn Assam what he wanted as reward.

"Sire, just grant me a single grain of wheat for the first square of this chessboard and two for the second and double it for each following square," answered Ibn Assam. The king thought this a modest reward for the health of his elephant. He told his servant to bring a bag of wheat. The servant put a grain of wheat on the first field, two on the second, four on the third, eight on the fourth, sixteen on the fifth, thirty-two on the sixth, and still the king was smiling. The servant went on and soon another bag of grain had to be brought and another and another. The king was not smiling anymore.

To fill the chess board with the promised grain the king would need $2^{65} - 1$ grains or over sixty-three million times the world's production of wheat in 1999. This problem was first posed by Ibn Kallikan, a 13th century mathematician. It has since been used in many tales like the one above. Exponential growth didn't ruin only the king. It is also one of the challenges for computational physics.

Many interesting problems are disordered and have a complicated energy landscape. Imagine you want to find the lowest valley in the Rocky Mountains by randomly wandering through the valleys and mountains. It is much easier to stay in a valley than cross a mountain so you will tend to spend a lot of time in one valley to make sure you didn't miss a spot before you'll climb up the next mountain. Finding the ground state of a spin glass is such a problem.

A spin glass is a system of spins that can be either up or down. The interaction between two spins either wants to align or antialign them. Often a spin is frustrated. It wants to be both up and down due to its neighbors. The time it takes to find a solution increases exponentially like the number of grains on the chessboard. If the solution for 4 spins can be found in a few seconds, the solution for 16 spins might already take several hours.

The spin glass belongs to a group of problems that in computer science is known as Nondeterministic Polynomial or NP. A solution for NP problems may be hard to find but is easy to test. Other problems in this class are the Traveling Salesman or the Vertex Cover problem. Many of these problems are important in practice. Imagine, for example, you want to protect a computer network from viruses by filtering traffic between computers (Fig. 1.1). The virus protection program should be installed on the smallest number of systems possible to minimize overhead. To be effective every connection between computers has to be covered, i.e., at least one of the computers connected must have the virus protection program. This problem is equivalent to finding the minimum vertex cover in the network graph in Fig. 1.2. The computers are the vertices and the connections are the

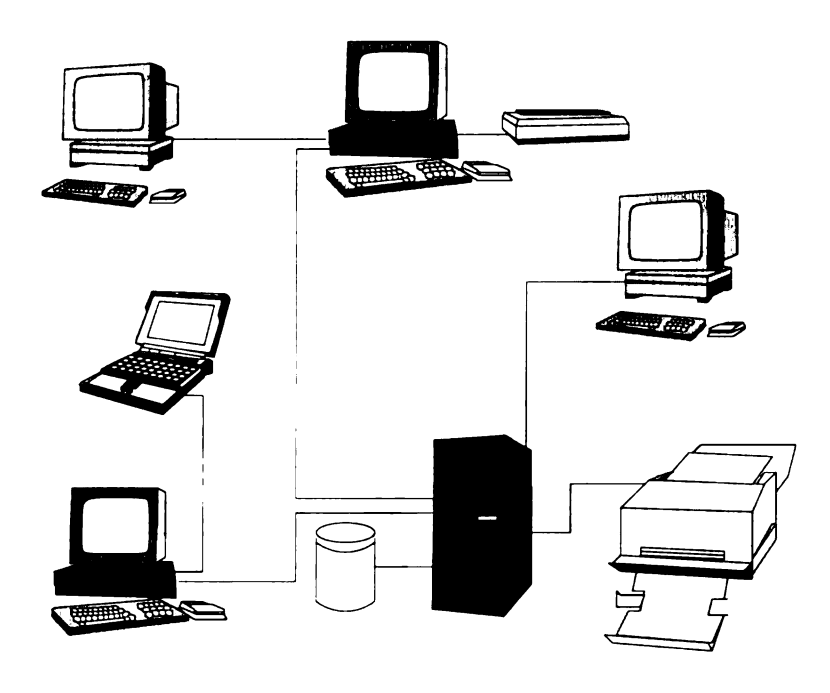


Figure 1.1: Computer network

edges.

The complement of the minimum vertex cover is the *maximal independent set*. It consists of those nodes that do not share any edges. In Fig. 1.2 the filled dots mark the vertex cover. The unfilled nodes are the corresponding independent set, which is equivalent to a lattice gas [57].

Recently the minimum vertex cover and other NP problems have attracted the interest of physicists. Using methods from statistical physics they find a phase transition. This phase transition, indicated by a critical slowing down of the computation, separates easy instances of the problem class from hard instances [21, 56, 57, 58].

Polynomial problems P can be solved efficiently. The time to find a solution scales with the system size, i.e., $t \sim N^x$ where N is the system size. A subset of NP problems can be mapped onto each other via polynomial algorithms. The subset is called NP-complete. NP-complete problems are among the hardest problems in computer science. As more and more problems are added to this class it is becoming increasingly unlikely that somebody will find an efficient way of solving them. One hope is that quantum computing will provide

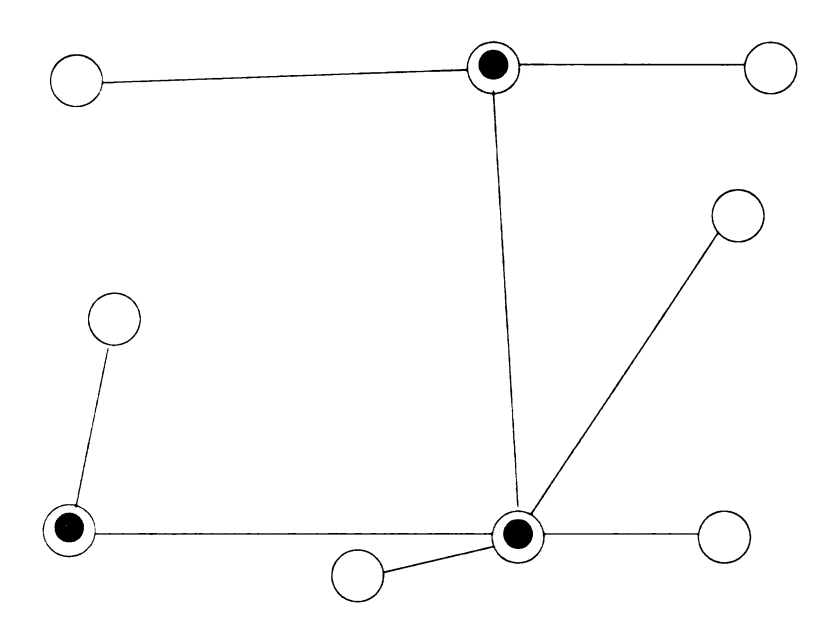


Figure 1.2: Network graph for computer network in Fig. 1.1. The filled dots mark a possible vertex cover.

new and efficient algorithms, but so far no polynomial quantum algorithm for NP-complete problems has been published. But *if* we find an efficient solution to any NP-complete problem, all NP-complete problems are polynomial. All polynomial problems are also NP problems since their solution can be checked in polynomial time. The question if *all* problems in NP are also in P is still open. The Clay Mathematics Institute named this question one of the seven Millennium Prize Problems and allocated one million dollars to the answer for each of the seven questions [12, 43].

Often there are sub-classes of NP problems that can be solved efficiently. For example, the spin glass in 2D can be solved by matching [3]. Other problems may seem hard for a long time until a new way of solving them is discovered. Among these is the random-field Ising model. In addition to the spin-spin interaction of the spin glass, it contains local random fields at each site. The interactions, however, are all ferromagnetic and want to align neighboring spins. The energy landscape of the random-field Ising model is very complex. At first Monte Carlo simulations were used to find the lowest energy state.

Monte Carlo simulations work like the traveler that wants to find the lowest lying valley

in the Rockies. It wanders through the energy landscape by changing the orientation of a spin at random and checking if the energy is lower. If the energy is lower, the change is accepted; if it is higher, the change is accepted with some probability depending on the temperature. The time the algorithm needs to find the global minimum increases exponentially with the system size and it gets harder and harder as the temperature approaches zero. In 1986 Ogielski published a revolutionary paper [39] where he solved the T=0K ($\approx -273^{\circ}C$) random-field Ising model using a polynomial algorithm: the maximum flow algorithm.

The maximum flow algorithm finds the maximum flow from a source to a target in a graph. This graph could represent the streets of a city, a network of water pipes, or the Internet. Each edge in the graph has a capacity, e.g., the number of cars that can pass through a street segment per minute.

As we have all experienced, it doesn't matter how wide a freeway is if there is a road construction that limits the traffic to one lane. This bottleneck determines how many cars can get through. In fact it can be proven that the maximum flow is exactly equal to the capacity of the bottleneck, the minimum cut. The geometry of the minimum cut can still be complex but that does not slow the algorithm down.

I used the maximum flow algorithm to study the ground state properties of the randomfield Ising model as well as the minimum energy fracture surface in polycrystalline materials. In both cases the minimum cut is the interface in the system.

The random-field Ising model is an important model for the study of complex system. It also models diluted antiferromagnets in a field, which play an important role in modern magnetic storage devices. The critical point of a phase transition is key to understanding the transition. The behavior near the critical point is often independent of the details of the system. Only the dimensionality and the symmetry of the order parameter matter. This is called universality. For the random-field Ising model the disorder critical point is the width

of the random distribution of random fields at which the magnetization goes to zero because the system becomes disordered. Many expected the random-field Ising model transition to be universal, but the matter is still debated. Phil Duxbury and I showed that for an infinite-range random-field Ising model the approach of the magnetization to zero is not universal. In the infinite-range model spins don't just interact with their neighbors, but equally with all other spins. In computer science this is called a complete graph because all nodes and edges in the graph are present. In an infinite-range model all spins are equivalent. This makes finding the ground state much easier.

The spins are trying to fulfill two conditions. They want to align with all the other spins and they also want to align with their local field. Usually this is not possible for all spins. In the ordered phase some spins have to pay the price for not aligning with their local fields. Since all spins have equivalent spin-spin interactions, these are the spins with the weakest local field. Based on this argument we can set up an equation for the magnetization m and find its behavior near the critical point where m goes to zero. For a universal system the behavior does not depend on the distribution of random fields. We found a distribution, however, (see Fig. 1.3) that allowed us to obtain any behavior near the critical point (see Fig. 1.4). This nonuniversality does not extend to Cayley trees - another model that often can be solved analytically - nor to 3 dimensions. In 3D I used the maximum flow algorithm to find ground state configurations. The behavior of the magnetization near the critical point is the same for different distributions. The correlation length, a measure of how many spins have to act in concert, is, on the other hand, not universal. For distributions with large fields that can flip a spin by themselves, the correlation length is shorter than for distributions where many local fields have to act together to flip a small cluster.

We encounter polycrystalline materials all the time. Most metals are polycrystalline. Polycrystalline diamond films cover drill bits and the scanners in super markets. High-temperature superconductors are finding more and more applications, e.g., in MRI (Mag-

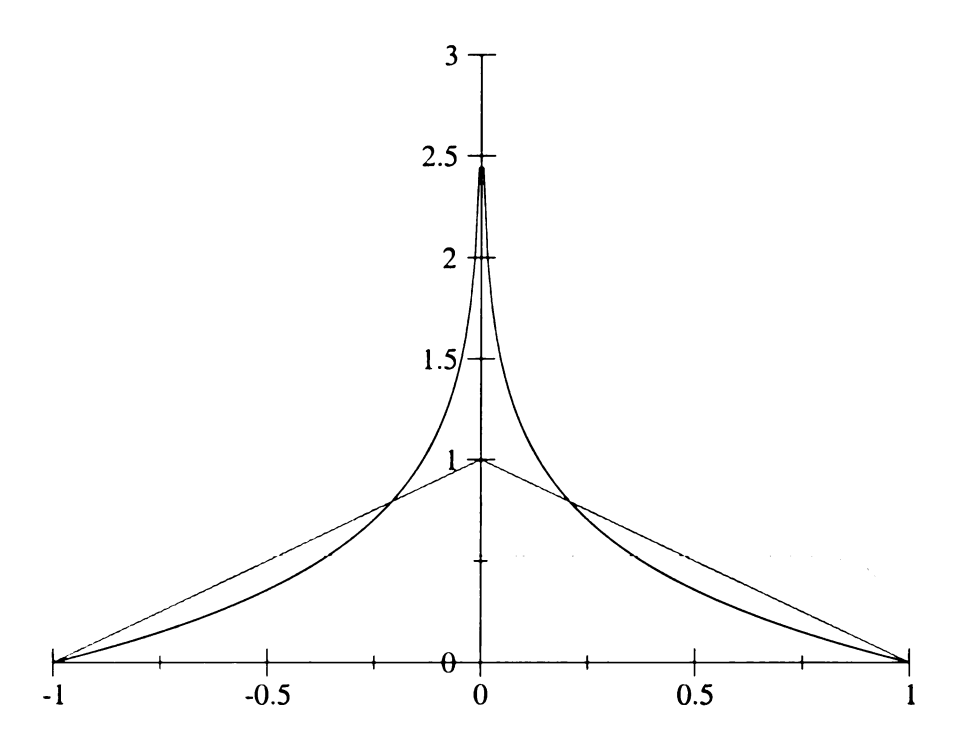


Figure 1.3: Tunable random distribution. $P(h) = \frac{y+1}{2Hy} \left(1 - \left(\frac{|h|}{H}\right)^y\right)$ for y=1/20 (top), 1 (middle), and 20 (bottom).

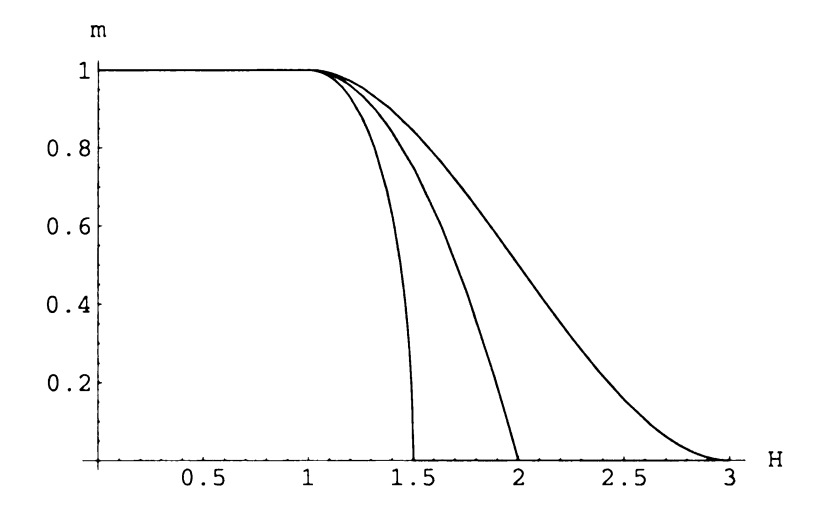


Figure 1.4: Magnetization for different distributions of random fields. This shows the magnetization for $P(h) = \frac{y+1}{2Hy} \left(1 - \left(\frac{|h|}{H}\right)^y\right)$ with y=2 (left), 1 (middle) and 1/2 (right)

netic Resonance Image) scanners and in the Maglev trains developed in Japan. High temperature superconductors are ceramics, which are by their very nature polycrystalline. We wanted to know how easily a polycrystal breaks, how rough its fracture surfaces are, and what the mechanism for roughening is. To study these properties we introduced two energy scales: the internal binding energy of the crystal grain and the adhesion energy. By varying the ratio of these two parameters we studied the roughness, energy, and location of the interface.

Roughening occurs on two length scales, locally and globally. The interface roughens locally by following grain boundaries that only deviate marginally from the straight cleavage line. This effect becomes stronger as the adhesion becomes weaker until the interface can follow any grain boundary at very weak adhesion.

To be in the lowest global energy state the interface must take advantage of fluctuations of the grain boundary angles. Some regions have a larger than average fraction of grain boundaries that are close to the cleavage direction, others have a smaller than average fraction of low angle grain boundaries. To take advantage of the low angle regions and avoid the large angle ones, the interface has to wander. These mechanisms combine to give an accurate description of our simulation data.

As we increase the average grain size the interface becomes increasingly rough. But it doesn't do it randomly. In 2 dimensions the roughness increases with the third root of the average grain size. Physicists call this a power law behavior because it can be written as roughness proportional to g to the one third power or $w \sim g^{1/3}$. Many quantities follow power laws. The energy necessary to form the interface, for example, increases with the d-1 power of the system size: $E \sim L^{d-1}$. d is the dimensionality of the system.

The behavior with respect to the adhesion energy is not as simple. For weak adhesion (adhesion/binding energy < 1/2) the interface stays rough. As the adhesion becomes stronger and stronger the interface becomes flatter. It becomes less favorable to go around

the grain. Recalling the mountain picture from before: once the hills become flat enough it's not worth going around them anymore. The interface cleaves the grain rather than taking the long way.

When the adhesion and grain binding energies are almost equal, the interface is flat on large length scales. This length scale is often called a critical length. The interface has to be at least as long as the critical length before you can tell that it is not flat.

The approach to flatter and flatter interfaces does not follow simple power laws. We can, however, make approximations near the point where the two energies are equal that give a good description of the behavior in terms of power laws. The energy, for example, increases linearly as we approach this point. Other quantities depend on the distribution of angles of grain boundaries within the sample.

Chapter 2

Analytic Methods and Concepts

Whenever physicists encounter a new problem they try to develop a model that is as simple as possible but still captures the essential features of the system. Often these models are one or two dimensional cases, or mean field theory, which corresponds to infinite dimensions. For thermal phase transitions these cases often give insight into the qualitative behavior in three dimensions. But sometimes they can be deceiving.

Best known - if not best understood - is the phase transition of water. At low temperature $(T < 0^{\circ}\text{C})$ water is a solid called ice. As temperature increases it melts and turns liquid. At temperatures above 100°C it starts boiling and becomes a gas. The solid-liquid and

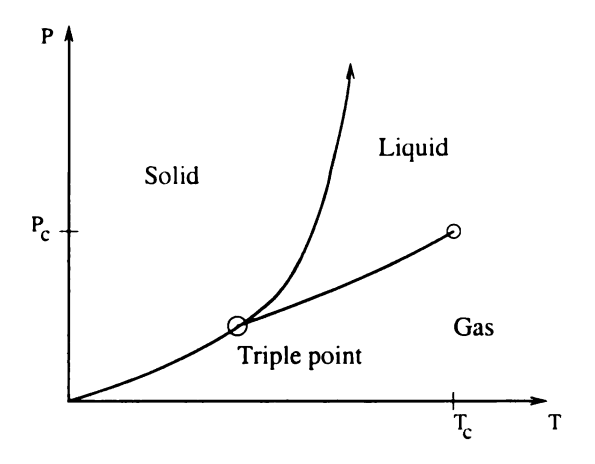


Figure 2.1: Phase diagram of water (cf. [48])

solid-gas transitions are example of first order phase transitions. The liquid-gas transition is second order above P_c and T_c . The characteristic feature of first order transitions is that the phases can coexist. In a second order transition, on the other hand, the two phases are indistinguishable at the transition point.

2.1 Critical exponents and scaling theory

To capture the nature of a phase transition we define an order parameter. This could, for example, be the difference in volume between the liquid and the gas phase for a liquid-gas transition or the magnetization for a ferro- to paramagnetic transition. The order parameter is chosen in such a way as to be zero at the phase transition [53].

We characterize the phase transition by the behavior of the order parameter near the critical point. More explicitly, one introduces a power law

$$f(x) = \begin{cases} f_0^+ * x^{-\lambda_f}, & x > 0\\ f_0^- * x^{-\lambda_f'}, & x < 0 \end{cases}$$

where λ_f is the *critical exponent* of the function f with respect to x for x > 0 and λ_f' is the critical exponent for x < 0. In practice there are often higher order corrections needed to accurately describe f(x). Therefore an alternate definition of the critical exponent is frequently used:

$$\lambda_f = \lim_{x \to 0} \frac{\ln f(x)}{\ln(-x)}.$$
 (2.1)

In this definition all correction terms vanish in the limit. It has, in addition, a very practical interpretation. The critical exponent is the slope of f(x) near the origin in a log-log plot.

In many cases the critical exponents do not depend on the details of the system under study but only on the symmetry of the order parameter, the spatial dimension, and the range

Symbol	Description	Definiton	Mean Field
α	Specific heat exponent	$C \sim \left(\frac{T-T_c}{T_c}\right)^{-\alpha}$	0
β	Magnetization exponent	$m \sim \left(\frac{T-T_c}{T_c}\right)^{\beta}$	$\frac{1}{2}$
γ	Susceptibility exponent	$\chi_T \sim \left(\frac{T-T_c}{T_c}\right)^{-\gamma}$	1
δ	Critical isothermal exponent	$M \sim H^{\frac{1}{\delta}}$	3
ν	Correlation length exponent	$\xi \sim \left \frac{(T-T_c)}{T_c} \right ^{-\nu}$	$\frac{1}{2}$

Table 2.1: The standard set of critical thermal exponents

of the interactions. This is called universality.

Several exponents denoted by a set of Greek letters are commonly used. The most important for my thesis are the magnetization exponent β and the correlation length exponent ν . For a summary of exponents and their definitions see Table 2.1.

The critical exponents are not all independent of each other. Some of the relations follow immediately from thermodynamics; others require additional assumptions about the scaling behavior of thermodynamical functions. I will use the scaling hypothesis to derive some of these relations.

An important function in statistical physics is the partition function (or "Zustandsfunktion", lit. function of state), which describes the system. A system is considered solved if there exists a solution for the partition function. It is defined as

$$Z = \sum_{\{\text{all states}\}} \exp(-\beta \mathcal{H})$$
 (2.2)

where $\beta = 1/(kT)$. k is the Boltzmann constant $(1.38 * 10^{-23} J/K)$. T is the temperature in Kelvin and \mathcal{H} is the Hamiltonian.

From Z we can obtain the free energy

Free energy,
$$F = -kT \ln Z$$
 (2.3)

and the relevant derivatives:

Magnetization,
$$M = -\frac{\partial F}{\partial H}$$
 (2.4)

Susceptibility,
$$\chi = \frac{1}{V} \frac{\partial M}{\partial H}$$
 (2.5)

Internal energy,
$$U = F - T \frac{\partial F}{\partial T}$$
 (2.6)

Heat capacity,
$$C = T^2 \frac{\partial^2 F}{\partial T^2}$$
 (2.7)

2.1.1 The scaling hypothesis

There are two approaches to the scaling hypothesis. The first one is motivated by the physical argument that sufficiently close to the phase transition the correlation length, ξ , is the only relevant length scale. A simple dimensional analysis leads to the scaling laws (see, e.g., [25]).

The second approach is more mathematical in nature and assumes that thermodynamic functions are homogeneous functions. A function is homogeneous if

$$\forall r \ f(\lambda r) = g(\lambda) f(r)$$

where g is limited to the form $g=\lambda^p$ with p the degree of homogeneity. This expression can be generalized to multiple independent variables, $f(\lambda x, \lambda y) = \lambda^p f(x, y)$ or even slightly more general

$$f(\lambda^a x, \lambda^b y) = \lambda f(x, y). \tag{2.8}$$

Note that this is the *most* general form of this equation. It cannot be further generalized by adding an exponent on the right hand side.

Now assume that the free energy defined in Eq. (2.3) is a homogeneous function

$$F(\lambda^{a_{\epsilon}} \epsilon, \lambda^{a_{H}} H) = \lambda F(\epsilon, H)$$
(2.9)

where $\epsilon = (T - T_c)/T_c$. Following Stanley's treatment [48], differentiate both sides of the Eq. (2.9) with respect to H

$$\lambda^{a_H} \partial F(\lambda^a \epsilon, \lambda^{a_H} H) / \partial H = \lambda \partial F(\epsilon, H) / \partial H.$$

Since $\partial F/\partial H=-M$ (cf. Eq. (2.4)) this is equivalent to

$$-\lambda^{a_H} M(\lambda^a \epsilon, \lambda^{a_H} H) = \lambda M(\epsilon, H). \tag{2.10}$$

There are two exponents associated with the magnetization (see Table 2.1) , β and δ . To get β set H=0 and let $\epsilon \to 0$, then Eq. (2.10) becomes

$$M(\epsilon, 0) = \lambda^{a_H - 1} M(\lambda^{a_\epsilon} \epsilon, 0). \tag{2.11}$$

Since Eq. (2.11) holds true for all values of λ it must be valid for $\lambda = (-1/\epsilon)^{1/a_{\epsilon}}$. Therefore

$$M(\epsilon,0) = (-\epsilon)^{(1-a_H)/a_\epsilon} M(-1,0)$$

and from the definition of the magnetization exponent we have

$$\beta = \frac{1 - a_H}{a_{\epsilon}}.$$

Similarly to obtain δ set $\epsilon = 0$ and let $H \to 0$,

$$M(0, H) = \lambda^{a_H - 1} M(0, \lambda^{a_H} H).$$

Choosing $\lambda = H^{-1/a_H}$ this becomes

$$M(0, H) = H^{(1-a_H)/a_H} M(0, 1)$$

and from the definition of δ we have

$$\delta = \frac{a_H}{1 - a_H}. (2.12)$$

The remaining exponents can also be related to the unknown scaling parameters a_{ϵ} and a_{H} . For example differentiating Eq. (2.9) twice with respect to H we obtain, using Eq. (2.5),

$$\lambda^{2a_H}\chi(\lambda^{a_\epsilon}\epsilon,\lambda^{a_H}H)=\lambda\chi(\epsilon,H).$$

For H=0 and $\lambda=(-\epsilon)^{-1/a_\epsilon}$ this becomes

$$\chi = (-\epsilon)^{-(2a_H - 1)/a_\epsilon} \chi(-1, 0)$$

for $\epsilon \to 0$ using the definition of γ

$$\gamma = \frac{2a_H - 1}{a_\epsilon}.\tag{2.13}$$

Now there are three different exponents defined by two unknowns. Expressing $a_{\it H}$ and

 a_{ϵ} in terms of β and δ one can rewrite γ as

$$\gamma = \beta(\delta - 1). \tag{2.14}$$

This is known as the *Widom equality*. The Widom equality can be rigorously derived as an inequality from thermodynamic relations. That it is satisfied as an equality is a prediction of the scaling hypothesis.

Similarly differentiating Eq. (2.9) twice with respect to ϵ leads to

$$\lambda^{2a_{\epsilon}}C(\lambda^{a_{\epsilon}}\epsilon,\lambda^{a_{H}}H) = \lambda C(\epsilon,H).$$

Again, since this equation is true for all λ it has to hold for the particular choice of $\lambda = (1/\epsilon)^{1/a_{\epsilon}}$. Setting H = 0,

$$\left(\frac{1}{\epsilon}\right)^{(2a_{\epsilon}-1)/a_{\epsilon}}C(1,0)=C(\epsilon,0).$$

From the definition of α ,

$$\alpha = \frac{2a_{\epsilon} - 1}{a_{\epsilon}}.\tag{2.15}$$

Combining Eqns. (2.12), (2.13), and (2.15) one obtains

$$\alpha + 2\beta + \gamma = 2,\tag{2.16}$$

which is known as the Rushbrooke equality.

As mentioned earlier, another way of deriving scaling relations is through dimensional analysis. First note that F/kT is dimensionless and F/kTV is therefore of dimension

γ	=	$\beta(\delta-1)$	Widom equality
2	=	$\alpha + 2\beta + \gamma$	Rushbrooke equality
2	=	$\alpha + \beta(1+\delta)$	Griffiths equality
$d\nu$	=	$2-\alpha$	Josephson law

Table 2.2: Scaling relations between the critical exponents.

length^{-d}. ξ is the only relevant length scale near the critical point, thus

$$\frac{F}{kTV} \sim \xi^{-\nu d}.$$

Comparing this with the definition of α we see that

$$2 - \alpha = \nu d. \tag{2.17}$$

Eq. (2.17) is called the *Josephson law*. Scaling relations that include dimension are often called hyperscaling relations.

Other relations can be derived in similar ways. Table 2.2 lists some of the more important ones.

2.2 Ising model

The Ising model was introduced by W. Lenz in 1920 [36]. He suggested it to his student E. Ising as his Ph.D. thesis topic. Ising solved the 1D Ising model as part of his thesis in 1924 [29] and the result was published in 1925 [30].

To their great disappointment they did not find a phase transition except at T=0K. For any finite temperature the 1D Ising model is a paramagnet. This was surprising since the importance of dimensionality for phase transitions had not been discovered yet.

Although introduced by his adviser the name "Ising Model" stuck. The term seems to have first been coined by R. Peierls in 1936 [40] (see [35] and references therein).

The Ising model is a two state system with ferromagnetic interactions between sites, i.e., neighboring sites prefer to be in the same state. Commonly it is viewed as a spin system where each spin can take only two values, $s=\pm 1$. The Hamiltonian is

$$\mathcal{H} = -\sum_{ij} J_{ij} s_i s_j \tag{2.18}$$

Finding the partition function for the 1 dimensional chain is beautifully simple. To ease notation let $J_{ii+1} \to J_i$. The partition function is then

$$Z = \sum_{\{s_1 = \pm 1\}} \sum_{\{s_2 = \pm 1\}} \cdots \sum_{\{s_N = \pm 1\}} \exp(\beta \sum_{i=1}^{N-1} J_i s_i s_{i+1})$$

$$= \sum_{\{s_1 = \pm 1\}} \sum_{\{s_2 = \pm 1\}} \cdots \sum_{\{s_{N-1} = \pm 1\}} \exp(\beta \sum_{i=1}^{N-2} J_i s_i s_{i+1}) \cosh(\beta J_{N-1} s_i).$$

Since \cosh is an even function the sign of s_{N-1} does not matter and one gets

$$Z = \sum_{\{s_1 = \pm 1\}} \sum_{\{s_2 = \pm 1\}} \cdots \sum_{\{s_{N-1} = \pm 1\}} \exp(\beta \sum_{i=1}^{N-2} J_i s_i s_{i+1}) 2 \cosh(\beta J_{N-1})$$

$$= \sum_{\{s_1 = \pm 1\}} \prod_{i=1}^{N-1} 2 \cosh(\beta J_i)$$

where the last sum just contributes another factor of two. The partition function is thus

$$Z = 2^N \prod_{i=1}^{N-1} \cosh(\beta J_i)$$

or for the case of uniform J,

$$Z = 2^N \cosh^{N-1}(\beta J).$$

To find the critical point for the magnetization without field, it is useful to analyze the

spin-spin correlation function $\Gamma(r)$.

$$\Gamma_k(r) = \langle s_k s_{k+r} \rangle$$

where

$$\langle s_k s_{k+r} \rangle = \frac{1}{Z} \sum_{\{s\}} s_k s_{k+r} \exp(-\beta \sum_{i=1}^{N-1} J_i s_i s_{i+1}).$$
 (2.19)

The sum over $\{s\}$ stands for the sum over all states. The above formula takes advantage of the fact that the average of any observable x can be calculated as

$$\langle x \rangle = \frac{1}{Z} \sum_{\text{all states}} x \exp(-\beta \mathcal{H}).$$

For r = 1 Eq. (2.19) becomes

$$\langle s_k s_{k+1} \rangle = \frac{1}{Z} \sum_{\{s\}} s_k s_{k+1} \exp(-\beta \sum_{i=1}^{N-1} J_i s_i s_{i+1})$$
$$= \frac{1}{Z} \sum_{\{s\}} \frac{\partial}{\partial J_k} \exp(-\beta \sum_{i=1}^{N-1} J_i s_i s_{i+1})$$
$$= \frac{1}{Z} \frac{\partial}{\partial J_k} Z.$$

For r=2 it is almost the same. Note that s_ks_{k+2} can be written as $s_ks_{k+1}s_{k+1}s_{k+2}$, thus

$$\langle s_k s_{k+2} \rangle = \frac{1}{Z} \sum_{\{s\}} s_k s_{k+1} s_{k+1} s_{k+2} \exp(-\beta \sum_{i=1}^{N-1} J_i s_i s_{i+1})$$

$$= \frac{1}{Z} \sum_{\{s\}} \frac{\partial}{\partial J_k} \frac{\partial}{\partial J_{k+1}} \exp(-\beta \sum_{i=1}^{N-1} J_i s_i s_{i+1})$$

$$= \frac{1}{Z} \frac{\partial}{\partial J_k} \frac{\partial}{\partial J_{k+1}} Z.$$

This can be generalized for any r to

$$\langle s_k s_{k+r} \rangle = \frac{1}{Z} \frac{\partial}{\partial J_k} \cdots \frac{\partial}{\partial J_{k+r-1}} Z.$$

For the case $s = \pm 1$ this is

$$\langle s_k s_{k+r} \rangle = \prod_{i=1}^r \tanh \beta J_{k+i-1}. \tag{2.20}$$

When does long range order set in? For long range order the following must hold true

$$\lim_{r \to \infty} \langle s_k s_{k+r} \rangle > 0.$$

The hyperbolic tangent is less than one for any finite argument. The product in Eq. (2.20) therefore goes to zero at any finite temperature. But, when $T=0 \Rightarrow \beta=\infty \Rightarrow \tanh\beta J=1$ so that at T=0K, the magnetization jumps from 0 to 1.

The solution for the 1D Ising model chain in an external field can be found using the transfer matrix method, which also forms the basis for the solution of the 2D Ising model without external field. The 2D Ising model does have a finite temperature phase transition at $T_c = 2.269 J/k$ [25].

For higher dimensions or for the 2D case with field, no exact solution has been presented so far. There are, however, many approximations and numerical methods that can provide insight into the nature of the phase transition.

2.2.1 Mean field theory

In mean field theory the interaction between spins is approximated by an effective field proportional to the average magnetization. It is therefore useful to first solve the non-

interacting spin system in a field. The Hamiltonian is

$$\mathcal{H} = -H\sum_{i} s_{i}.$$

The partition function is

$$Z = \sum_{\{s_i = \pm 1\}} \exp(\beta H \sum_i s_i)$$
$$= 2^N \cosh^N \beta H.$$

The free energy is $F = -kT \ln Z$ and the magnetization $M = -(\partial F/\partial H)_T$,

$$M = \frac{\partial}{\partial H} kT \ln Z$$

$$= kT \frac{\beta 2^{N} N \cosh^{N-1} \beta H \sinh \beta H}{2^{N} \cosh^{N} \beta H}$$

$$= N \tanh \beta H$$

$$m = \frac{M}{M_0} = \tanh \beta H$$

In mean field theory, the effective field is $H_{\rm eff}=H+\lambda m$, where λ is called the molecular field parameter. Replacing H by $H_{\rm eff}$ we get

$$m = \tanh \beta (H + \lambda m). \tag{2.21}$$

Eq. (2.21) is an implicit equation. For H=0 it can easily be solved graphically (see Fig. 2.2). The figure shows that m=0 is always a solution and that there are non trivial solutions only if the slope of $\tanh(\beta \lambda m)$ at m=0 is greater than 1. To determine when

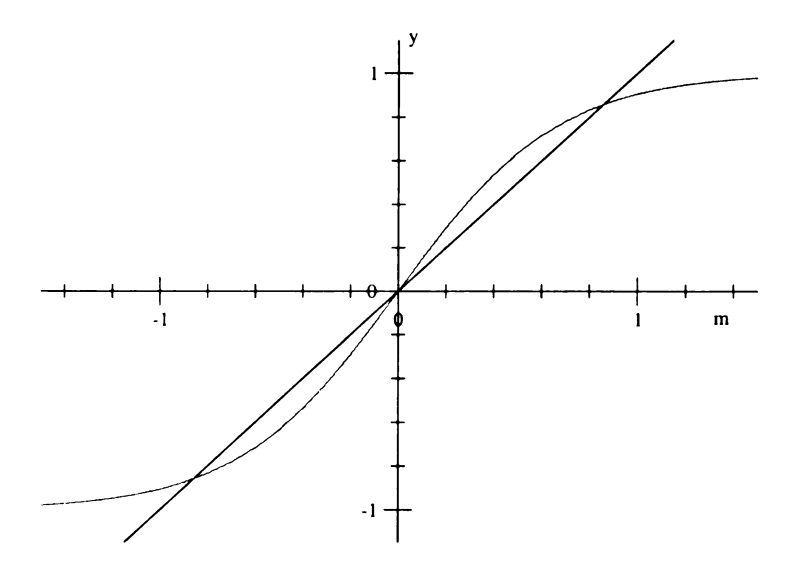


Figure 2.2: Graphical solution of the magnetization in mean field theory. The solution of Eq. (2.21) is the intersection of the two graphs. In the above plot $\lambda=1.5$. For $\lambda<1$ only m=0 remains a solution.

this is the case expand the right hand side of Eq. (2.21) to first order around 0.

$$\tanh(\beta \lambda m) \simeq \beta \lambda m + \mathcal{O}((\beta \lambda m)^3)$$

$$\Rightarrow \lambda \beta > 1 \Leftrightarrow \frac{\lambda}{kT} > 1$$

$$\Leftrightarrow \frac{\lambda}{k} > T$$

$$T_c = \frac{\lambda}{k}. (2.22)$$

To find the critical exponent for the magnetization β introduce $\tilde{T} = \frac{T}{T_c} = \frac{k}{\lambda}T$ and expand the right hand side of Eq. (2.21) around 0.

$$m = \frac{m}{\tilde{T}} + \frac{1}{3} \frac{m^3}{\tilde{T}^3} + \cdots$$

$$m^2 \simeq 3 \left(1 - \frac{1}{\tilde{T}} \right) \tilde{T}^3$$

$$\simeq 3 \tilde{T}^2 (\tilde{T} - 1)$$

$$\simeq 3 \left(\frac{T}{T_c} \right)^2 \left(\frac{T - T_c}{T_c} \right),$$

thus

$$m \sim \left(\frac{T - T_c}{T_c}\right)^{1/2}$$

so that $\beta = 1/2$.

2.2.2 Infinite range model

In 1968 Kac showed [33] that mean field theory can be interpreted as a system with infinite range interaction. For the Ising model the infinite range Hamiltonian is

$$\mathcal{H} = -\frac{J}{N} \left(\sum_{i} s_{i} \right)^{2} + J. \tag{2.23}$$

The partition function is

$$Z_N = \sum_{\{s_i\}} \exp(\beta(J/N) \left(\sum_i s_i\right)^2 + \beta J)$$
$$= e^{\beta J} \sum_{\{s_i\}} \exp(\beta J/N \left(\sum_i s_i\right)^2).$$

Using the identity

$$\int_{-\infty}^{\infty} \exp(-ax^2 + bx) = \sqrt{\pi/a} \exp(b^2/4a)$$
 (2.24)

with $a=N/4J\beta$ and $b^2=\left(\sum_i s_i\right)^2$ the partition function can now be written as

$$Z_{N} = e^{\beta J} \sum_{\{s_{i}\}} \int_{-\infty}^{\infty} \exp(-\frac{N}{4J\beta}x^{2} + \sum_{i} s_{i}x) dx$$

$$= e^{\beta J} \int_{-\infty}^{\infty} \exp(-\frac{N}{4J\beta}x^{2}) \sum_{\{s_{i}\}} \exp(\sum_{i} s_{i}x) dx$$

$$= e^{\beta J} \int_{-\infty}^{\infty} \exp(-\frac{N}{4J\beta}x^{2}) 2^{N} \cosh^{N} x dx$$

At large x the first term of the integrand dominates. It is proportional to $\exp(x^2)$ whereas the second term only goes like $\exp(x)$. This suggests the saddle-point method, or method of steepest descent [48, 6]. In the saddle point method the integral is replaced

by the largest value of the integrand in the interval. The free energy is thus

$$F \approx -kT(\beta J + \ln \max_{-\infty \le x \le \infty} \exp(-\frac{N}{4J\beta}x^2) 2^N \cosh^N x)$$
 (2.25)

Since the logarithm is monotonically increasing we can find the maximum of the integrand by finding the maximum of the logarithm of the integrand.

$$f(x) = -\frac{N}{4\beta J}x^2 + N\ln(2\cosh x)$$
 (2.26)

$$f'(x) = -\frac{Nx}{2\beta J} + N\frac{2\sinh x}{2\cosh x}$$
$$= -\frac{Nx}{2\beta J} + N\tanh x$$

$$f'(x_e) = 0$$

$$0 = -\frac{Nx}{2\beta J} + N \tanh x$$

$$x = 2\beta J \tanh x$$

This is recognized as essentially the mean field equation for the magnetization with H=0 (cf. Eq. (2.21)).

2.2.3 Cayley tree

The Cayley tree, or Bethe lattice, is another solvable model that usually gives mean field-like behavior. To construct a Cayley tree start at a node 0 and add z neighbors. To each neighbor add z-1 neighbors and so on (see Fig. 2.3). Each interior node has z neighbors and each leaf node has only 1 neighbor. Often instead of z the number of children $\alpha = z - 1$ is

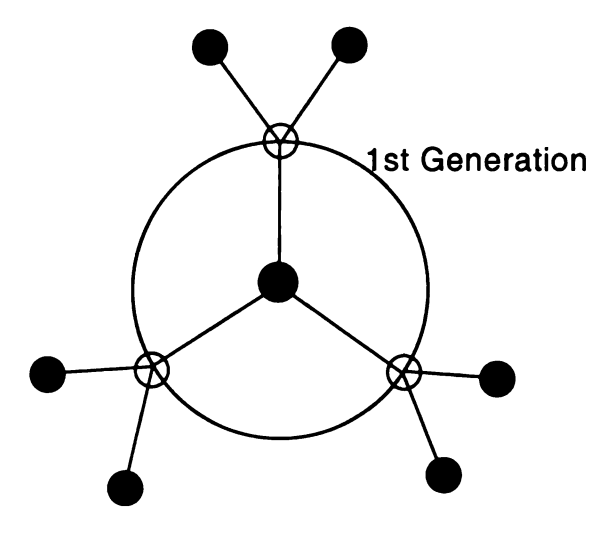


Figure 2.3: Cayley tree with z=3

used to describe the tree.

A Cayley tree with z=3 and 3 generations, for example, consists of 10 nodes of which 6 are on the surface. For larger and larger Cayley trees the ratio between the number of leaves, the nodes on the surface, and the total number of nodes goes to $(\alpha-1)/\alpha$ and not to zero as it does for more conventional lattices for $d<\infty$. In that respect the Cayley tree acts like an infinite dimensional lattice. For $z\to\infty$ it can be shown that the Cayley tree usually gives the same results as mean field theory.

2.2.4 Renormalization group and universality

In 1966 Kadanoff [34] presented an intuitive picture on how to rescale the Ising model. He suggested to successively group the spins in blocks with a volume b^d , where b is the length of the block and d is the dimension. Each block of spins is then assigned a spin, e. g., the average spin value with some spin chosen as tie breaker. Then the Hamiltonian is rewritten in terms of these "block spins". He considered only nearest neighbor interactions for the spins as well as the block spins. This technique is based on the idea that for distances

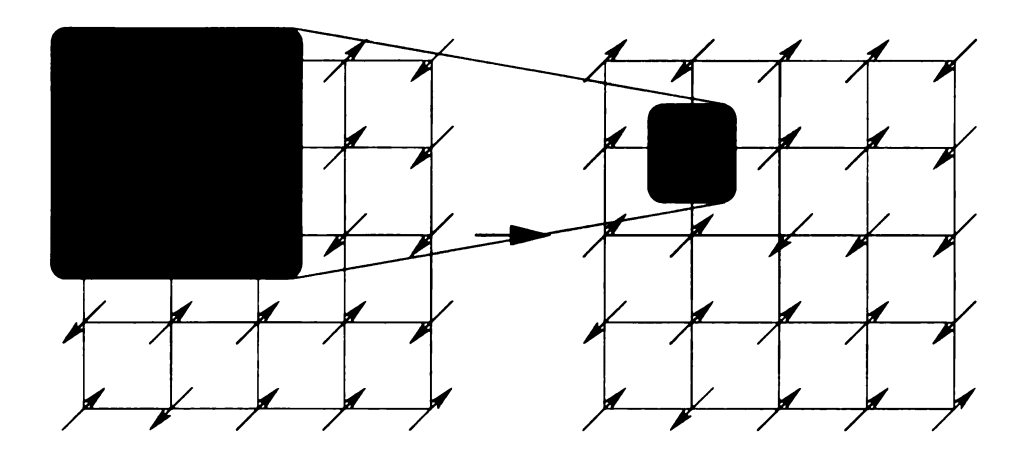


Figure 2.4: Kadanoff's block spins for an Ising model. The shaded 3x3 block of spins on the left becomes a single block spin on the right.

much smaller than the correlation length ξ the spins should act in concert. The method is illustrated in Fig. 2.4.

Although this method provides a nice visualization, the restriction to nearest neighbor interactions makes it all but useless for practical calculations. Thus it is necessary to include all possible interactions and write the Hamiltonian in its most general form.

$$\mathcal{H}(\mathbf{K}, \{s_i\}, N) = K_0 + K_1 \sum_{i} s_i + K_2 \sum_{ij^{(1)}} s_i s_j + K_3 \sum_{ij^{(2)}} s_i s_j + K_4 \sum_{ijk^{(1)}} s_i s_j s_k + \dots$$

where the (n) at the indices indicates summation only over the $n^{\rm th}$ nearest neighbors. The partition function is thus

$$Z(\mathbf{K}, N) = \sum_{\{s_i\}} \exp(-\mathcal{H}(\mathbf{K}, \{s_i\}, N)).$$

Now introduce blocks and sum over the spins inside the block σ_i .

$$Z(\mathbf{K}, N) = \sum_{s_I, \sigma_I} \exp(-\mathcal{H}(\mathbf{K}, \{s_I, \sigma_I\}, N))$$
$$= \sum_{\{s_I\}} \exp(-\mathcal{H}(\mathbf{K}_L, \{s_I\}, NL^{-d})).$$

Note that the partition function in terms of the block spins has the same form as the original partition function. K and K_L are related by the transformation

$$\mathbf{K}_L = \mathbf{T}(\mathbf{K}).$$

Since the Hamiltonian has the same form as before, the process can be repeated for larger and larger blocks.

$$\mathbf{K}_{nL} = \mathbf{T}(\mathbf{K}_{(n-1)L}) \tag{2.27}$$

If the system is not at the critical point, the correlation length ξ will get smaller and smaller with each successive rescaling. Therefore the system moves further and further away from criticality. If the system is critical, however, ξ remains infinite. The transformation T can no longer change K. For such values K^* ,

$$\mathbf{K}^* = \mathbf{T}(\mathbf{K}^*). \tag{2.28}$$

T is called the renormalization group although it is only physically relevant as a semi-group since the inverse of T, the unblocking of block spins, has no physical interpretation. K^* is called a fixed point of the transformation.

To learn more about the behavior of the system near a fixed point subtract (2.28) from (2.27),

$$\mathbf{K}_{nL} - \mathbf{K}^* = \mathbf{R}(\mathbf{K}_{(n-1)L}) - \mathbf{K}^*.$$

For $n \gg 1$ one can make the linear approximation

$$\mathbf{R}(\mathbf{K}_{nL}) = \mathbf{R}(\mathbf{K}^*) + \mathbf{W}(\mathbf{K}_{nL} - \mathbf{K}^*)$$

where W is a matrix with the elements

$$\mathbf{W}_{\alpha\beta} = \left. \frac{\partial R_{\alpha}}{\partial K_{\beta}} \right|_{\mathbf{K} = \mathbf{K}^{\bullet}}.$$

The eigenvectors of \mathbf{W} \mathbf{u}_{α} can be used to represent the coupling-constant vector \mathbf{K}_{nL} . The new coordinates are

$$\mathbf{v}_{nL} = \sum_{\alpha} \mathbf{u}_{\alpha} (\mathbf{K}_{nL} - \mathbf{K}^*)_{\alpha}.$$

The eigenvalues λ_{α} determine the behavior of the associated coordinate under renormalization group transformation. For $\lambda_{\alpha} < 1$ the coordinate moves towards the critical point. For $\lambda_{\alpha} > 1$ the coordinate moves away from criticality. The critical surface in \mathbf{K} space is defined by $v_{\alpha} = 0$ for all $\lambda_{\alpha} > 1$ with \mathbf{K}^* as the origin. All systems with \mathbf{K} in the critical plane will approach the same fixed point under successive renormalization group transformations and belong to the same universality class and have the same critical exponents [42, 25]. Often the latter part of the previous statement is used to define a universality class: Systems that show the same critical behavior and thus have the same critical exponents belong to the same universality class.

2.3 Landau theory

Landau theory tries to express phenomenologically the behavior of a system near its critical point. It only deals with macroscopic quantities and explicitly avoids microscopic details. Nevertheless it has been very successful, and offers yet another insightful way to the mean field approximation. I will follow Huang's introduction to the Landau approach [25].

Starting with a macroscopic system in d dimensions assume that there exists some coarse grained order parameter density, m(x). Coarse graining could be done by averaging over some volume a^d . Then there are no fluctuations in m(x) on length scales shorter than

a. Therefore there are no Fourier components with wave number greater than $\Lambda \sim 1/a$. The partition function can be written as

$$Z(H,T) = \exp(-G(H,T)/kT) = N \int \exp(-E(m,H))(Dm)$$
 (2.29)

where G is the Gibbs free energy and E is

$$E(m,H) = \int dx \psi (m(x), H(x)).$$

The integral in Eq. (2.29) is a functional integral over all possible forms of m(x) that do not vary over a.

 $\psi(m(x), H(x))$ is called the *Landau free energy*. Near the critical point where m(x) is small it can be expanded in powers of m(x):

$$\psi(m(x), H(x)) = \frac{1}{2} |\nabla m(x)|^2 - \frac{1}{kT} m(x) H(x) + \frac{1}{2} r_0 m^2(x) + s_0 m^3(x) + u_0 m^4(x) + \cdots$$

where r_0 , s_0 , u_0 are parameters that may depend on temperature and Λ . u_0 is usually considered independent of temperature while r_0 is of the form

$$r_0 = a_0 \epsilon$$

with a_0 positive and $\epsilon = (T - T_c)/T_c$.

The simplest approximation to the functional integral in Eq. (2.29) is the saddle point approximation [6]. The integral is replaced by the maximum value of its integrand. This approximation leads to mean field theory. For constant H, $m(x) = \bar{m}(H,T)$ with the

boundary conditions

$$\left. \frac{\partial \psi(m,H)}{\partial m} \right|_{m=\bar{m}} = 0 \tag{2.30}$$

$$\left. \frac{\partial^2 \psi(m, H)}{\partial m^2} \right|_{m = \bar{m}} \ge 0 \tag{2.31}$$

maximizes the integrand. The Landau free energy in the mean field approximation expanded in powers of m is

$$\psi(m,H) = \frac{mH}{kT} + \frac{1}{2}r_0m^2 + s_0m^3 + u_0m^4 + \cdots$$

From ψ one can calculate the Gibbs free energy

$$\frac{1}{V}G(H,T) = kT\psi(\bar{m},0) - \bar{m}H$$

and the magnetization $M=-\partial G/\partial H$

$$\frac{M}{V} = \bar{m}.$$

Choose

$$\psi(m, H) = \frac{1}{2}r_0m^2 + u_0m^4 - \frac{mH}{kT}$$

where $u_0>0$ and $r_0=a_0\epsilon$. From Eq. (2.30) we have

$$r_0\bar{m} + 4u_0\bar{m}^3 - \frac{H}{kT} = 0. {(2.32)}$$

For H=0, $\bar{m}=0$ is always a solution and

$$a_0\epsilon = -4u_0\bar{m}^2.$$

Additional real solutions exist only for $\epsilon < 0$. They are

$$\bar{m} = \pm \sqrt{\left(a_0/4u_0\right)|t|}$$

which gives $\beta = 1/2$.

The magnetic susceptibility is obtained by differentiating \bar{m} with respect to H. From Eq. (2.32) we get

$$\chi = \frac{1}{kT(r_0 + 12u_0\bar{m}^2)}$$

and $\gamma = 1$. All the other exponents listed in Table 2.1 take on their mean field values, too.

2.4 Percolation

So far I have used thermal phase transitions to introduce the concepts of critical phenomena. This is, however, not the only situation where critical phenomena arise. Another class of systems experiences criticality due to quenched randomness. Quenched here means that the disorder changes - if at all - on a time scale much larger than that of thermal fluctuations.

One such system is percolation. Percolation comes in two flavors: bond percolation and site percolation. In both cases we consider a regular lattice in d dimensions. In bond percolation all sites in the lattice are present and we add one *bond* at a time. The question is then, at which concentration of bonds, $p = p_c$, does a path appear that connects opposite sides of the lattice. In other words, when does a path percolate from one side of the lattice to the opposite one. The concentration of bonds at that point gives the percolation threshold. For small p only a few bonds (or edges) are present. Therefore only small clusters of nodes connected by edges can form. As p increases, larger and larger clusters begin to form until, finally, there is a percolating cluster (see Fig. 2.5). The percolating cluster is also called the infinite cluster since its size is of order the system size and becomes infinite in the

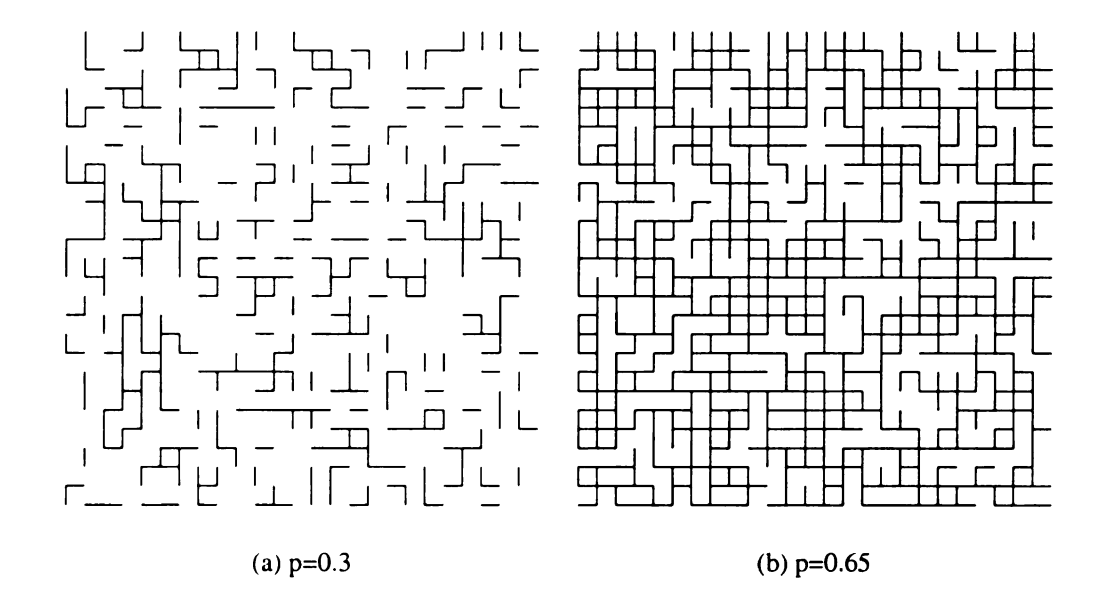


Figure 2.5: Percolation on a square lattice. The left graph shows a square lattice with a bond concentration p=0.3. There is no percolating path. The right graph has a concentration of p=0.65 where most bonds are part of the percolating cluster.

thermodynamic limit, i.e., in the limit of infinite system size.

For site percolation imagine a checker board. One square at a time is occupied and the question becomes at which concentration, $p = p_c$, of occupied squares does a path containing only occupied squares appear that percolates.

The order parameter in percolation is the probability P of a node to be part of the infinite cluster. For $p < p_c$, P is 0 since there is no infinite cluster. Above p_c the probability increases until it becomes 1 at p = 1. Two other quantities are of interest: the average cluster size $\langle s \rangle$ and the finite cluster size distribution n_s [49, 4].

The average cluster size $\langle s \rangle$ is defined as

$$\langle s \rangle = \sum_{s=1}^{\infty} P_p(s) s$$

where $P_p(s)$ is the probability to have a cluster of size s at a concentration p. The cluster size distribution, or normalized cluster number n_s , is defined as the number of clusters of

size s per lattice site:

$$n_s = \frac{1}{s} P_p(s).$$

I have not related percolation to disorder so far. To remedy this, let all bonds (sites) have a randomly assigned value between 0 and 1. Usually the random numbers are drawn from a uniform distribution. For a particular value of p all bonds (sites) with a value less than p are present (occupied).

To get a better feel for the above quantities let us first look at the one dimensional chain. Any hole in the chain interrupts the percolating cluster thus $p_c = 1$. The probability to be on the infinite cluster P is 0 for $p < p_c$ and 1 for $p = p_c$. Assume L is large so that we can ignore the ends of the chain. To get a cluster of size 1 the site has to be occupied, which it is with probability p, and its two neighbors have to be empty. The probability for a site to be empty is 1 - p. Since we assume independent random variables the probability for any two sites to be empty is just $(1 - p)^2$. The probability of having a cluster of size 1 per lattice site is thus $n_1 = p(1 - p)^2$. For a cluster of size 2, 2 neighboring sites have to be occupied and the ends have to empty. This gives $n_2 = p^2(1 - p)^2$. Or for a cluster of size s

$$n_s = p^s (1 - p)^2.$$

Next let us look at the correlation function $\Gamma(r)$. The correlation function gives the probability of two sites at a distance r to belong to the same cluster. For r=0, $\Gamma(0)=1$. For r>0 all sites between the origin and the site at distance r have to be present, which happens with probability p^r .

$$\Gamma(r)=p^r.$$

For $p < p_c$, $\Gamma(r)$ goes to zero exponentially,

$$\Gamma(r) = e^{-r/\xi},$$

where ξ is the correlation length.

$$\xi = -\frac{1}{\ln(p)}$$

or near the critical point

$$\xi = -\frac{1}{(p_c - p)},$$

which in analogy to the thermal case leads to a critical exponent $\nu = 1$ (see Table 2.1).

2.4.1 Cayley tree

For another exactly solvable example consider the Cayley tree. Just like described earlier each site is assigned a value between 0 and 1 drawn from a uniform distribution. A site is occupied if its value is less than p.

We consider percolation from the origin to the surface. For a percolating path to exist at least one of the (z-1) (or z for the origin) neighbors has to be present. Therefore $p(z-1) \ge 1$ and the percolation threshold is

$$p_c = \frac{1}{z - 1}. (2.33)$$

This time $p > p_c$ is accessible and we can study the behavior of P, the probability of a site to be part of the infinite cluster, in more detail.

Even above p_c there is no guarantee that the origin or any other node is part of the infinite cluster. All neighboring sites could be unoccupied. This happens with a probability of $(1-p)^z$. Even if all neighbors are present it is possible for none of the neighbors to be connected to the surface. Let Q be the probability that a branch is not connected to the surface. For simplicity consider z=3. The probability that neither of the sub branches lead to infinity is Q^2 . The probability that the neighbor site is occupied but none of its sub branches are connected to infinity is pQ^2 . The probability that the neighbor is missing

already is 1 - p. Thus the total probability for a branch not to lead to infinity because either the neighbor is missing or neither of the sub branches lead to infinity is

$$Q = (1 - p) + pQ^2. (2.34)$$

Equation (2.34) has two solutions: $Q_1 = 1$ and

$$Q_2 = \frac{1-p}{p}.$$

The probability that the origin is not part of the infinite cluster is $p-P=pQ^3$, which leads to P=0 for Q_1 corresponding to $p< p_c$ and

$$\frac{P}{p} = 1 - \left(\frac{1-p}{p}\right)^3$$

for Q_2 corresponding to $p \geq p_c$.

To make the recursive nature of the calculation more explicit I can write the probability of a site at level l+1 to be connected to the surface in terms of the probabilities at level l. The level count starts from the surface.

$$P(l+1) = p \sum_{g=1}^{\alpha} \begin{pmatrix} \alpha \\ g \end{pmatrix} P^g(l) Q^{\alpha-g}(l).$$

Just like in the previous calculation I find the steady state solution by setting $P(l) = P(l + 1) = P^* = (1 - Q^*)$,

$$P^* = p \sum_{g=1}^{\alpha} \begin{pmatrix} \alpha \\ g \end{pmatrix} P^{*g} (1 - P^*)^{\alpha - g}. \tag{2.35}$$

If the sum started at zero Eq. (2.35) would be a binomial sum of the form

$$\sum_{g=0}^{\alpha} \begin{pmatrix} \alpha \\ g \end{pmatrix} P^{*g} (1 - P^*)^{\alpha - g} = (P^* + (1 - P^*))^{\alpha}.$$

Thus we can rewrite Eq. (2.35) as

$$\frac{P^*}{p} = (P^* + (1 - P^*))^{\alpha} - (1 - P^*)^{\alpha}.$$

For $\alpha = 2$ this is

$$\frac{P^*}{p} = (P^* + (1 - P^*))^2 - (1 - P^*)^2$$
$$= P^{*2} + 2P^*(1 - P^*)$$
$$0 = (2 - \frac{1}{p})P^* - P^{*2}.$$

The first solution is $P^* = 0$, which corresponds to p < 1/2. The second solution is

$$P^* = (2 - \frac{1}{p}).$$

For the central spin the probabilities of the $z=\alpha+1$ incoming branches have to be combined. The probability for the central spin to be connected to the surface is

$$P_{0} = p \sum_{g=1}^{z} \begin{pmatrix} \alpha \\ g \end{pmatrix} P^{*g} (1 - P^{*})^{\alpha - g}$$

$$\frac{P_{0}}{p} = (P^{*} + (1 - P^{*}))^{z} - (1 - P^{*})^{z},$$

which for $\alpha = 2$, $z = \alpha + 1 = 3$ becomes

$$\frac{P_0}{p} = P^{*3} + 3P^{*2}(1 - P^*) + 3P^*(1 - P^*)^2$$
$$= 1 - \left(\frac{1 - p}{p}\right)^3.$$

The second way of finding P looks more complicated than the first one but is easier to extend as I'll show later.

2.4.2 Giant clusters in random graphs

The definition of percolation that I gave above contained a regular lattice in some dimension where neighboring nodes are connected with edges. It may seem odd at first to extend percolation to a system where neighbors can be infinitely far away and a percolating cluster can consist of one edge and two nodes. Although the connectivity aspect is the intuitive interpretation of percolation, I defined all the quantities, including the order parameter, in terms of clusters and cluster sizes. A cluster can exist in a random graph just as well as on a regular lattice. Random graphs have first been studied by Erdös and Rénya [16]. They are interesting to both mathematicians and physicists [4, 31].

A graph consists of nodes and edges connecting the nodes. In a complete graph every node is connected to every other node in the graph. Again assign a random number between 0 and 1 to each edge. A random graph with concentration p is a complete graph, where an edge is present if its value is less than p. Erdös noticed that for each property of the graph he investigated, for example, the emergence of trees of size 3 or the emergence of cycles, there exists a threshold. For p below this threshold almost no graphs have this property and for p above the threshold almost all graphs have this property. This included the emergence of the giant cluster. The giant cluster includes a finite fraction of the nodes. It is equivalent to the infinite cluster in percolation.

In contrast to percolation theory where p_c is independent of the system size the threshold in a random graph, which is an infinite dimensional system, depends on the system size and goes to either 0 or 1 for $N \to \infty$. Instead of using p directly, define an exponent z with $p(N) = N^z$. The critical values of z are independent of N.

In random graph theory often the evolution of graphs is considered. Starting from a graph with N nodes and no edges we slowly increase $p(N) = N^z$, the concentration of edges. z varies from $-\infty$, p(N) = 0, to 0, p(N) = 1. For z < -3/2 only isolated nodes and edges are present. At z = -3/2 trees of order 3 appear. For z = -1 the structure of the graph changes dramatically. The average connectivity < k >= 1, and a giant cluster forms containing of the order of $N^{2/3}$ nodes.

We can study the growth of the giant cluster using invasion percolation and Cayley trees. Pick a vertex v and label it as visited. All adjacent vertices are labeled active unless they have been visited already. Now pick an active vertex and repeat. If we use a first in-first out (FIFO) queue for the active vertices, this procedure grows a Cayley tree. The active vertices are the leaves of the tree and form the growth surface. The critical connectivity for the giant cluster is $\langle k \rangle = 1$ as for the Cayley tree in Sec. 2.4.1. The Cayley tree has, as I mentioned in Sec. 2.2.3, properties that one usually only finds in an infinite dimensional system. I can therefore use it as a model for infinite dimensional percolation. The appearance of the giant cluster in a random graph and percolation in infinite dimension are therefore in the same universality class.

Chapter 3

Paths, Domain Walls, and Spin Clusters in Random Media

Flux lines in super conductors, directed polymers in random media, domain walls in the 2D random-bond Ising model, shortest paths in networks are all examples of directed paths in physics. They find their way through complex energy landscapes and often stick to pinning sites or random pinning areas caused by fluctuations. Pinning and the complex energy landscape make it very hard to find the global minimum for any of these paths. Simulated annealing methods get stuck around the pinning sites, which are deep local minima, and it takes a long time to overcome those large barriers to explore other parts of the energy landscape.

The problem becomes even more difficult as we move to higher dimensions. Domain walls in the 3D random-bond Ising model are surfaces with additional degrees of freedom. In the random-field Ising model more than one domain can form so that there is a multitude of possible configurations. Often we use the term *manifolds* instead of paths and surfaces.

Finding the global minimum for manifolds in random media is a hard problem due to local minima that have almost the same energy as the global minimum but are often far

away in space. In 1986, however, Ogielski [39] presented results for the ground state of the random-field Ising Model at T=0K that he obtained using an algorithm from combinatorial optimization. This opened the door to detailed, large scale investigations of disordered Ising models.

3.1 Domain walls and random bonds

The random-bond Ising model (RBIM) is the most general form of the Ising model without field as introduced in 2.2. The Hamiltonian is given by Eq. (2.18),

$$\mathcal{H} = -\sum_{ij} J_{ij} s_i s_j,$$

where, as the name implies, each bond can have a random bond strength J_{ij} .

If we fix the boundary spins to be up on one side and down on the opposite side, two domains will form. For uniform J the interface between the two domains is flat. A flat interface minimizes the number of neighbors with opposite spins and therefore the energy cost of creating the boundary. There is no preferred location for this interface either. It is degenerate. In a two dimensional system the interface is a path, in three it's a surface.

In a random-bond model it may be favorable to break more but weaker bonds and thus form a rough interface.

The roughness and energy are independent of the distribution, P(J) [26, 17]. The roughness scales as

$$w = \sqrt{\langle h^2 \rangle - \langle h \rangle^2} = b_1 L^{\zeta},$$

with $\zeta = 2/3$ in two and $\zeta = 0.41(1)$ in three dimensions. The energy scales as

$$E = a_1 L^{d-1} + a_2 L^{\theta}$$

with $\theta = 1/3$ in 2D and $\theta = 0.82(2)$ in 3D [38, 2].

3.2 Spin clusters and random fields

The random-field Ising model (RFIM) is the most general form of an Ising model with ferromagnetic interactions. A random field is associated with each spin. The fields are drawn from some distribution, P(h), where h can be positive or negative. In addition the spin-spin interaction can be non-uniform and a uniform external field can be present. The full Hamiltonian for the RFIM is

$$\mathcal{H} = -\sum_{ij} J_{ij} s_i s_j - \sum_i s_i (h_i + B). \tag{3.1}$$

The RFIM has an order-disorder transition depending on the width of the random distribution in d>2. For a long time this was a hotly debated topic. Imry and Ma [28] gave a simple argument that identified d=2 as the critical dimension and predicted a phase transition in 3D. From renormalization group arguments, however, it was predicted that the behavior of a disordered system should be the same as the ordered system in d-2. Thus there should be no phase transition in 3D. In 1984 Imbrie showed rigorously [27] that there is a phase transition in 3D but none in 2D.

Numerical simulations weren't of much help either. The energy landscape of the RFIM has many local minima. Monte Carlo simulations easily get stuck in these minima. The transfer matrix method is another algorithm that was employed early in RFIM calculations. Both Monte Carlo and the transfer matrix method are exponential algorithms. The maximum time needed by these algorithms to find the solution increases exponentially with the system size. But in 1986 Ogielski published numerical results using for the first time a mapping of the problem of finding the ground state in the RFIM to the maximum flow problem of combinatorial optimization [39]. The mapping provides exact ground states at

T=0K in polynomial time. This allowed Ogielski and others to study larger systems and get better statistics. The two major questions that Ogielski addressed are, however, still under debate: Is the phase transition first or second order in 3D and is it universal, i.e., does the phase transition depend on the random distribution.

The latter point is important for practical reasons. The closest experimental realization of the RFIM is the diluted antiferromagnet in a field (DAFF). It is supposed to be in the same universality class as the random-field Ising model. But if the phase transition of the RFIM is not universal, which distribution has to be used to compare it with the experimental results?

Chapter 4

Maximum Flow/Minimum Cut

All the problems treated in my thesis have some instances where finding the ground state can be mapped to finding the minimum cut in a capacitated network.

Combinatorial optimization provides us with efficient ways to find the minimum cut by using maximum flow algorithms. The maximum flow is equal to the capacity of the minimum cut.

In this chapter, after presenting and proving the maximum flow/minimum cut theorem, I detail various mappings to the relevant physics problems. Finally I explain two algorithms that solve the maximum flow problem.

4.1 The maximum flow/minimum cut theorem

Let G(V,E) be a graph where V is a set of vertices (or nodes) and $E \subseteq V \times V$ a set of edges. Each edge has a capacity u and a flow f. The maximum flow problem can then be phrased as follows: Given a set of sources $\{s\}$ and a set of sinks $\{t\}$ find the maximum amount of flow that can be transported from $\{s\}$ to $\{t\}$ subject to the constraints

$$\forall v \in V \setminus (\{s\} \cup \{t\}) : \sum_{w} f(w, v) = \sum_{w} f(v, w) \tag{4.1}$$

$$\forall e \in E : f_e \le u_e. \tag{4.2}$$

A flow that obeys Eq. (4.1) and (4.2) is considered a *feasible flow*. For the remainder of this chapter I will consider only one source s and one sink t unless otherwise noted.

A cut is a set of edges separating V in two disjoint sets S and T, $V = S \cup T$. If s is in S and t is in T the cut is called an s-t cut. The capacity of such a cut is given by

$$u(S,T) = \sum_{v \in S.w \in T} u(v,w).$$

The cut with the minimum capacity u(S,T) is the minimum cut. Its capacity gives an upper bound for the flow. Actually, it can be shown that the maximum flow is exactly equal to the minimum cut. This is known as the maximum flow/minimum cut theorem [3, 32].

PROOF: Adding the balance constraint (Eq. (4.1)) for all nodes in S and doing the same for all nodes in T we get

$$|f| = \sum_{v \in S} \left(\sum_{w} f(w, v) - \sum_{w} f(v, w) \right)$$
$$= \sum_{v \in T} \left(\sum_{w} f(v, w) - \sum_{w} f(w, v) \right)$$
$$= \sum_{(v, w) \in (S, T)} f(v, w) - \sum_{(v, w) \in (T, S)} f(v, w)$$

All flows within S cancel and the same is true for all flows within T. Only the flow between

S and T remains. Since $f_e \leq u_e$ and $f_e \geq 0$

$$|f| \le \sum_{(v,w)\in(S,T)} u(v,w) = u(S,T).$$

This means that any flow f is at most equal to the capacity of any cut (S,T). Therefore if we find a flow |f| that is equal to the capacity of a cut (S,T) we find the maximum flow and the minimum cut. \square

4.2 Mappings to the maximum flow/minimum cut problem

Several interesting ground state problems in physics map to the maximum flow/minimum cut problem.

4.2.1 Finding the interface in a random-bond Ising model with fixed boundaries

Historically the mapping for the random-bond Ising (RBIM) problem was discovered several years *after* the mapping of the ground-state random-field Ising model problem described in 4.2.2. But it is easier to visualize.

I want to find the interface in a random-bond Ising model where the spins of two of the boundaries are fixed to +1 and -1 respectively. The boundary conditions force two spin domains and therefore an interface. The Hamiltonian for the RBIM is (cf. 3.1)

$$\mathcal{H} = -\sum_{ij} J_{ij} s_i s_j,$$

with $J_{ij} \geq 0$.

Let V be the set of all spins. Then any spin configuration has a set of spins $S=\{i\in V|s_i=1\}$ and a set of spins $\overline{S}=\{i\in V|s_i=-1\}=V\setminus S$. The energy of such a system can be written as

$$E = -\sum_{(s_i \in S, s_j \in S)} |J_{ij}| - \sum_{(s_i \in \overline{S}, s_j \in \overline{S})} |J_{ij}| + \sum_{(s_i \in S, s_j \in \overline{S})} |J_{ij}|$$
(4.3)

$$= -\sum_{ij} |J_{ij}| + 2 \sum_{\substack{(s_i \in S, s_j \in \overline{S}) \\ E_{\text{opt}}}} |J_{ij}|$$

$$(4.4)$$

$$= E_{\rm opt} + 2E_{\rm interface.} \tag{4.5}$$

In the ground state E is minimal and therefore $E_{\rm interface}$ must be minimal since $E_{\rm opt}$ is always the same. The factor of 2 is needed since all bonds in the interface have already been counted in the optimal energy and this has to be canceled.

Let G be a graph. To map the random-bond Ising model interface to a graph problem, map each spin in V to a node in G. The interaction J_{ij} between two spins is represented by an edge between those spins. The capacity u_{ij} of this edge is equal to the strength of the interaction, $u_{ij} = J_{ij}$. To fix the boundaries introduce two ghost nodes, s and t, and connect all spins on one face to s using edges of infinite capacity and all spins on the opposite face to t again with edges of infinite capacity. Now find the maximum flow from s to t. The minimum cut will separate the system in two domains, one connected to s and one connected to s. All spins connected to s have $s_i=1$ and all spins connected to s have $s_i=1$.

As I showed in 4.1 the maximum flow is equal to the sum of capacities on the minimum cut

$$u_{\rm cut} = \sum_{i \in S, j \in \overline{S}} u_{ij}.$$

Using the definition of S and \overline{S} and the assignment of spins, this is exactly equal to

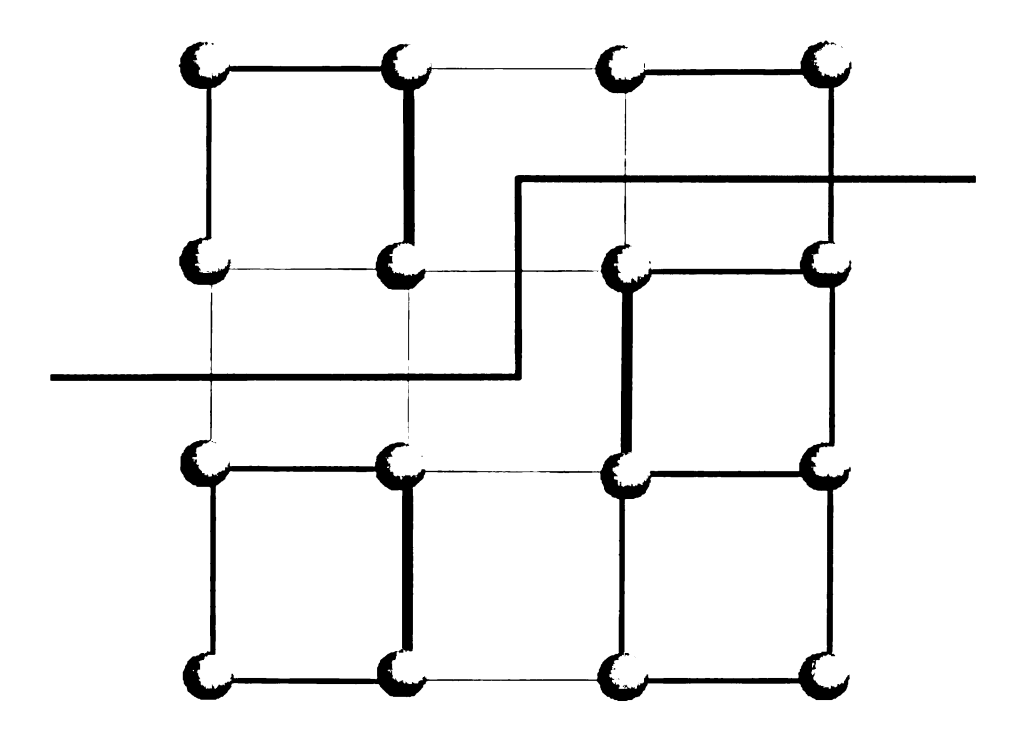


Figure 4.1: The minimum cut in a random-bond Ising model. The strength of the spin-spin interaction is indicated by the thickness of the line. The thick line crossing the sample shows the location of the minimum cut.

 $E_{\text{interface}}$.

4.2.2 The mapping of the random-field Ising model to the maximum flow/minimum cut problem

The mapping of the random-field Ising model (RFIM) is very similar to the one for the RBIM. In fact the RFIM can be treated as a special case of the RBIM. Again introduce two ghost nodes, s and t. Every site with a positive field is connected to s, and every site with a negative field to t. The capacity of each of these edges is equal to the magnitude of the field, i.e., $u_{si} = h_i$, and $u_{it} = |h_i|$. In this way the spin-field interaction is mapped into a spin-spin interaction and the Hamiltonian can be written as

$$\mathcal{H} = -\sum_{ij} u_{ij} s_i s_j,$$

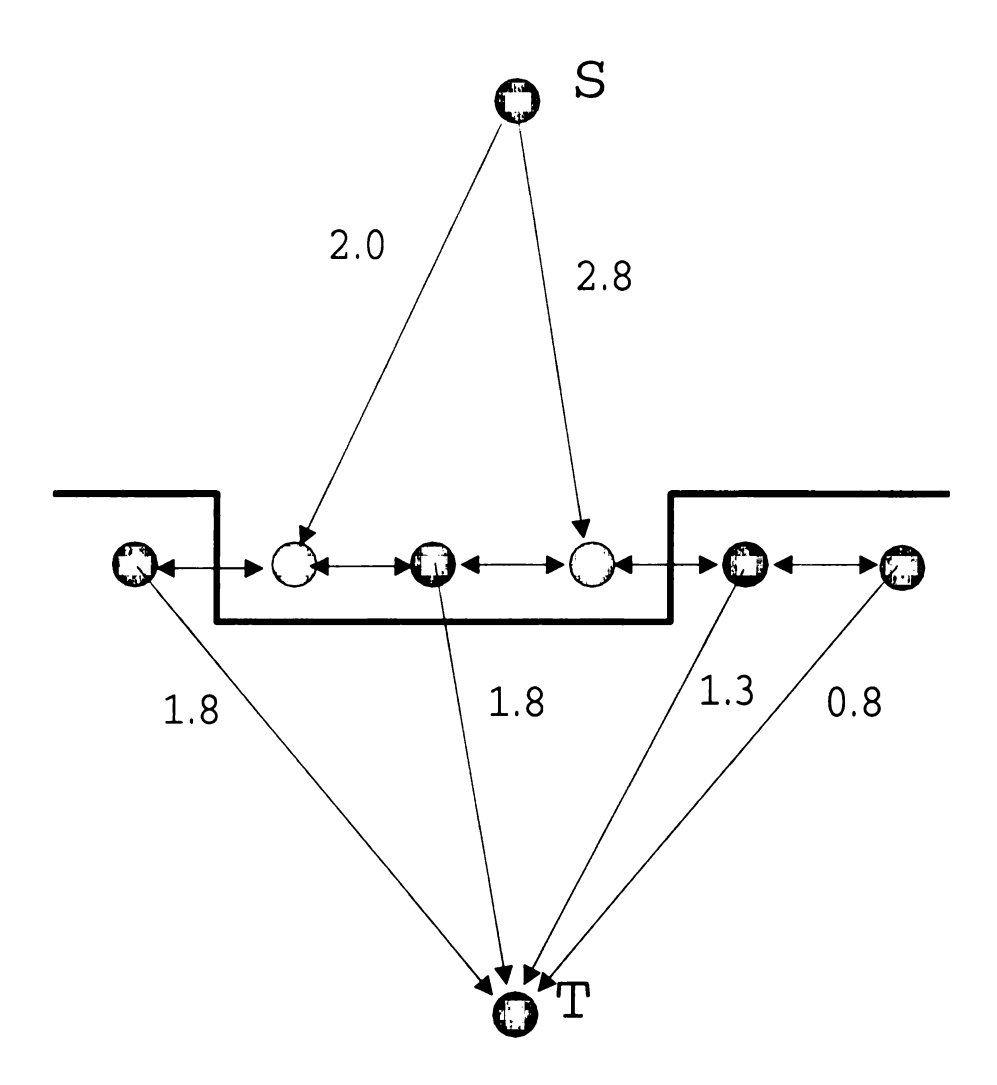


Figure 4.2: Mapping of a 1D random-field Ising model to the maximum flow problem. The source S is connected to the spins that have a local field pointing upwards. The sink T is connected to the spins where the random field is pointing downwards. The numbers give the magnitude of the fields in terms of J. The thick line indicates the minimum cut. All spins above the cut are up in the ground state. All spins below the cut are down.

where i and j run over $V \cup \{s, t\}$.

The minimum cut in this case is not limited to spin-spin bonds but can also include broken field bonds. The energy can be written exactly as in Eq. (4.5) with $S \to S \cup s$ and $\overline{S} \to \overline{S} \cup t$.

The geometry of the minimum cut in the RFIM, however, is completely different from the one in the RBIM. Instead of two domains separated by a single interface, there is a multitude of clusters with domain walls between them.

4.3 Algorithms for solving the maximum flow problem

4.3.1 The augmenting path algorithm

To check if a flow f is maximal it is sufficient to verify that there is no path from s to t along which the flow could be increased [32]. Such paths are called *augmenting paths*. Augmenting paths form the basis of our first algorithm (see Alg. 1).

Find an augmenting path from s to t. Determine the minimum capacity u_{min} on this path and send u_{min} units of flow from s to t. Calculate the *residual graph* and repeat the procedure until no more paths with $u_{min} > 0$ can be found. The excess on t is the maximum flow. The residual capacity of an edge e_{ij} is just $u_{ij}^r = u_{ij} - f_{ij} + f_{ji}$ where f_{ij} is the flow from node t to node t.

How fast is the algorithm? The complexity of an algorithm is expressed in the "big O" notation. Instead of using benchmark times that change with faster computers, the order of the number of operations is given in terms of the size of the system. Constant prefactors are usually ignored. Finding a path with residual capacity greater than zero can be done using a breadth first search (bfs) and takes $\mathcal{O}(|E|)$ operations where |E| is the number of edges. Augmenting the flow along the path takes $\mathcal{O}(|V|)$, the length of the path. Each time there is at least one critical edge that will be saturated on this path. Therefore this procedure

```
initialize
repeat
  # find augmenting path
  choose first unlabeled node v w/ pre(v)
  forall outgoing edges e of v:
      if NOT pre(w=tail(e)) AND f(e) < u(e):
         pre(w) = v
         dir(w) = +
         d(w) = \min(u(e) - f(e), d(v))
  forall incoming edges e of v:
     if NOT pre(w = head(e)) AND f(e) > 0:
         pre(w) = v
         dir(w) = -
         d(w) = \min(f(e), d(v))
  label v
  if pre(t):
     #augment flow
      w=t
      d=d(w)
      while w \neq s:
         v = pre(w)
         if dir(w) = +:
           f(e) = f(e) + d
         else:
           f(e) = f(e) - d
         w=v
      forall v in V except s:
         delete pre(v) and dir(v)
         d(v) = \infty
         clear label of v
```

main:

until all nodes v with pre(v) are labeled

Algorithm 1: Augmenting path algorithm by Edmonds and Karp (1972)

needs to be repeated a maximum of |E| times and the total complexity of the algorithm is $\mathcal{O}(|V||E|^2)$. For the typically sparse graphs in physics problems this reduces to $\mathcal{O}(|V|^3)$.

The augmenting path algorithm is representative of a class of flow algorithms that maintain a feasible flow at every step and strive towards an optimal solution. A flow is feasible if $f_{ij} \leq u_{ij}$ and for every node i, $\sum_j f_{ij} - f_{ji} = 0$, in other words the flow is conserved at each node and never larger than the maximum capacity of the edge.

4.3.2 Push-relabel

Another class of algorithms maintains a solution that is always optimal but not necessarily feasible at each step of the algorithm. Among these is the push-relabel algorithm by Goldberg and Tarjan [19]. Instead of finding one path from s to t at a time, *all* edges originating from s are flooded up to capacity at once. The result is an excess flow at the connected nodes. The excess flow is then pushed towards t or if that is not possible, back to the source. This procedure is repeated until all excess flow lies at either s or t (see Alg. 2).

The terms "towards t" and "back to the source" imply a direction and, thereby, a distance. In fact the push-relabel algorithm requires a valid distance label at each node. The distance label can change over time. A node can be raised so that its neighbors become accessible to push flow into them. A valid labeling scheme obeys the following rules: d(t) = 0, d(s) = N, $d(i) \le d(j) + 1$ for all i, j where $u_{ij}^r > 0$. Setting the distance of all nodes but s to zero is therefore a valid labeling. A reverse breadth first search starting at t, however, also gives a correct distance label and improves overall performance.

With the distance labels defined, it is now possible to give the rules for the push and relabel procedures. Given an active node i, active meaning a node with an excess flow $x_i > 0$, a push can be performed if there is an edge with $u_{ij}^r > 0$ and d(i) = d(j) + 1. This ensures that flow will be pushed towards the sink as long as possible. If a node i is active and all its neighbors have $d(i) \leq d(j)$ i gets relabeled $d(i) = \min\{d(j) + 1 | u_{ij}^r > 0\}$. At

first glance this might seem too restrictive. Due to the definition of u_{ij}^r , however, there is always the possibility to push the flow back to where it came from.

```
main:
    determine distance label
    forall outgoing edges i of s:
      f_{si} = u_{si}
      f_{is} = -f_{si}
      u_{si}^r = 0
      u_{is}^r = u_{is} + u_{si}
      x_i = f_{si}
    while there is an active node i:
      choose an active node i
       apply an allowed operation to i
push:
   if i is active AND r_{ij} > 0 AND d(i) == d(j) + 1:
      \delta = min(x_i, r_{ij})
      f_{ij} = f_{ij} + \delta
      f_{ji} = f_{ji} - \delta
      u_{ij}^r = u_{ij}^r - \delta
      u_{ii}^{r} = u_{ii}^{r} + \delta
      x_i = x_i - \delta
relabel:
   if i is active AND forall u_{ij}^r > 0 AND d(i) \le d(j):
      d(i) = \min(d(j) + 1|u_{ij}^r > 0)
```

Algorithm 2: Push-relabel algorithm by Goldberg and Tarjan

The order in which push and relabel operations are performed is important for the performance of the algorithm. Using a first-in-first-out (FIFO) queue of active nodes and repeating the push operation until the node is either no longer active or a relabel is necessary, it can be shown that the algorithm can be done in $\mathcal{O}(|V|^3)$ time. Further improvements using more complicated data structures are possible. The best bound for a push-relabel algorithm is currently $\mathcal{O}(|V||E|\log(|V|^2/|E|))$ [11, 19].

4.4 Benchmarks

For most of my calculations I took advantage of LEDA [37], a library written in C++ that provides many well implemented advanced data structures and algorithms. I also wrote my own library of graph data structures and algorithms, SmaGL, in C++. In this section I present some benchmark results for LEDA and SmaGL using Goldberg's implementation of his push-relabel algorithm in C as a reference. The benchmarks were performed on a Dual PIII Xeon 550MHz PC with 2GB of memory.

SmaGL uses the FIFO implementation described in 4.3.2. Both LEDA and Goldberg use a different ordering, the highest-label (HL) ordering. In the highest-label implementation the active node with the largest distance label is used next. Cherkassky and Goldberg [11] showed that the HL implementation is faster than FIFO for all tested problem instances. FIFO, however, is easier to implement, performs well, and is much easier to parallelize.

The benchmark consisted in calculating the interface in a random-bond Ising model (see 4.2.2) with opposing fixed boundaries in one, and open boundaries in the other directions, on a 3D cubic lattice. For each linear size L between 10 and 100 different samples were solved.

Note that although LEDA (squares) and Goldberg (diamonds) perform better in absolute times, SmaGL (circles) scales best (see Fig. 4.3).

In this chapter I proved the maximum flow/minimum cut theorem. I showed how to map the random-bond and the random-field Ising to a maximum flow problem. I presented the augmenting path and the push-relabel algorithm to solve the maximum flow problem. Finally, I gave some benchmark results for three implementations of the push-relabel algorithm.

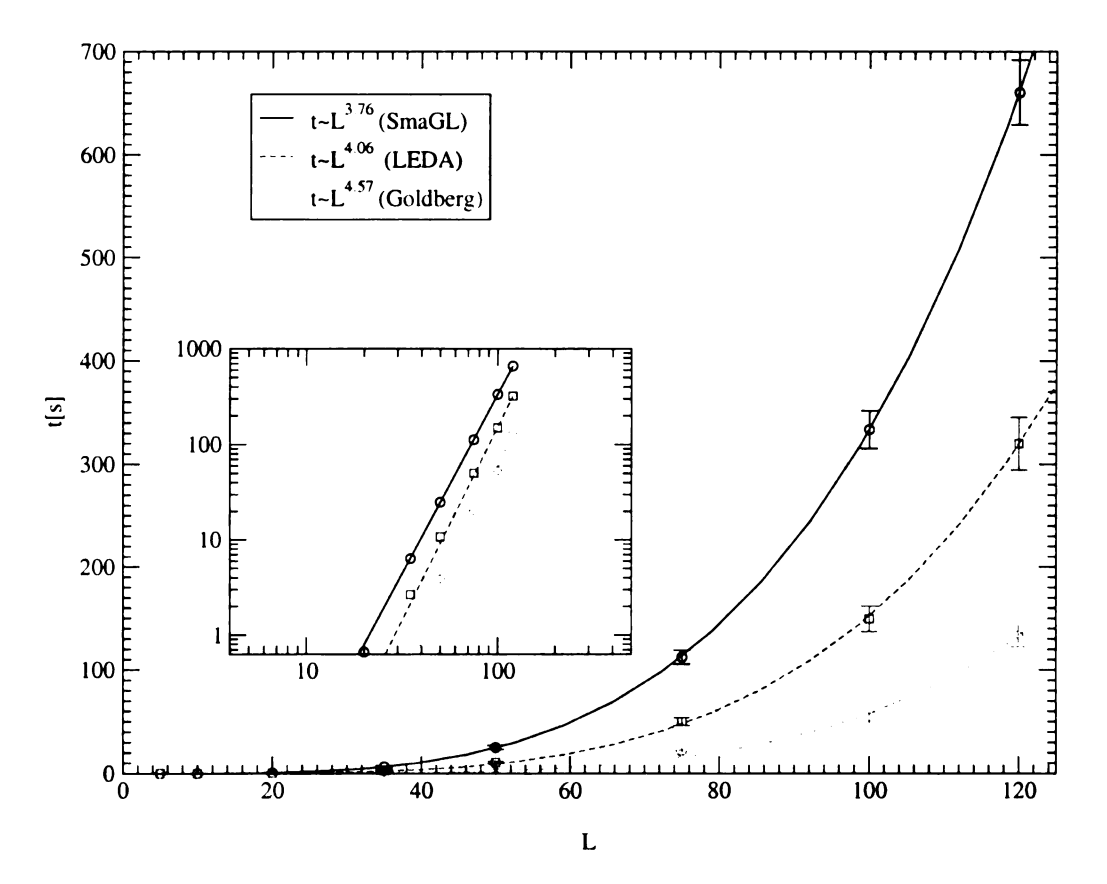


Figure 4.3: Push-relabel Benchmarks. The plot shows the time needed to solve the maximum flow problem for a random-bond Ising model for different system sizes for 3 different implementations (see text). The lines are best fits of the form $t=a*L^b$. The values for b are given in the legend. The inset shows the same data on a log-log plot.

Chapter 5

Random-Field Ising Model

The central issue in the equilibrium random-field Ising model (RFIM) is the nature of the phase transition from the ferromagnetic state at weak disorder to the frozen paramagnetic state at high disorder. The existence and universality class of the RFIM transition is key, as the best experimental tests of RFIM theory are diluted antiferromagnets in a field (DAFF), e.g., $Fe_{1-x}Zn_xF_2$, which are believed to be in the same universality class as the RFIM. In 1979 Fishman and Aharony showed [18] that a uniform magnetic field in a disordered anisotropic antiferromagnet creates random fields proportional to the external field. In $Fe_{1-x}Zn_xF_2$, Fe is replaced randomly by non-magnetic Zn atoms. This creates disorder and anisotropy. The external field is the control parameter that allows us to change the strength of the random effective fields and thus drive the system from an ordered antiferromagnet at low field to a paramagnet at high field.

After some controversy it was rigorously demonstrated [27] that the RFIM transition occurs at a finite threshold of the width of the distribution in three dimensions, and at an infinitesimal threshold in one and two dimensions. It seems natural to try to extend the idea of universality discussed in 2.1 to systems with quenched disorder. In fact several systems like percolation and directed polymers in a random medium (DPRM) show universal

properties. But in more complex systems, like spin glasses, universality, though often assumed, is unproven. Aharony showed [1] that already the mean field RFIM can behave in two distinct ways depending on the distribution of random fields. If the distribution has a maximum at the origin, the transition is second order with exponent 1/2. For distributions with a minimum at the origin he predicted a first order transition. Numerical studies at zero temperature suggest that in four dimensions the bimodal case is first order, and the Gaussian case is second order. The analysis in three dimensions is less conclusive [51]. The difference between the Gaussian and bimodal cases has been attributed to percolative effects [52]. Numerical work in three dimensions has also suggested that the correlation length exponent, as deduced from finite size scaling, is nonuniversal [13].

Another important concept for RFIM is the zero temperature fixed point. Renormalization group theory predicts that temperature is not a relevant parameter for phase transitions in the RFIM. Thus phase transitions can be studied at T=0K and the results should be applicable at finite temperature. This is of particular interest since there exists an *exact* mapping of the ground state of the RFIM to the minimum s-t cut problem from combinatorial optimization, which can be solved exactly in polynomial time (see Chapter 4).

5.1 Infinite-range random-field Ising model

Studying the infinite range random-field Ising Model (IRIM) at T=0K, Phil Duxbury and I find that the critical exponent for the magnetic phase transition can vary continuously depending on the distribution of random fields. This means that the RFIM is nonuniversal in the ground state. Furthermore, this behavior is not observed at any finite temperature where the usual thermal order parameter 1/2 is restored.

The Hamiltonian for the infinite-range random-field Ising model is

$$\mathcal{H} = -\frac{J}{N} \sum_{ij} s_i s_j - \sum_i h_i s_i$$

where the first sum is over all spin pairs and the second is over all spins. To find the ground state it is only necessary to minimize the Hamiltonian since entropy does not contribute to the free energy at T=0K. The minimum energy possible would be achieved with all spins aligned and all local fields pointing along the same direction. If the distribution is symmetric around zero, this is not feasible. There are additive terms due to broken spin-spin interactions and misaligned fields.

Given a particular magnetization m there is a number of spins $n_+ = N(1+m)/2$ pointing upwards and a number of down spins $n_- = N(1-m)/2$. Without loss of generality let m > 0. The exchange energy per spin is

$$E_x = -\frac{J}{2N^2}(n_+^2 + n_-^2 - 2n_+n_-) = \frac{-J}{2}m^2.$$

The field energy has two terms. The first represents the maximum possible field energy with all spins aligned with their fields

$$E_{h_0} = -\int_{-\infty}^{\infty} |h| P(h) dh.$$

The second term is due to misaligned fields. For the infinite range model all spins are equivalent. In the ground state the local misaligned fields will therefore be those with the smallest magnitude. The total field energy is thus

$$E_h = -\int_{-\infty}^{\infty} |h| P(h) dh + 2 \int_{0}^{h_c} h P(h) dh$$

where h_c depends on the magnetization and the distribution. Taking advantage of the symmetry of the distribution, h_c is defined by

$$\frac{n_{+}}{N} - \frac{1}{2} = \int_{0}^{h_{c}} P(h)dh.$$

I can rewrite the left hand side of the above equation in terms of the magnetization $m = 2(n_+/N) - 1$,

$$m = 2 \int_0^{h_c} P(h)dh. \tag{5.1}$$

To find the ground state I need to minimize the total energy. This is done in the usual way by setting the first derivative of the energy with respect to the magnetization to zero and then comparing the second derivative to zero.

$$\frac{\partial E}{\partial m} = -Jm + 2h_c P(h_c) \frac{\partial h_c}{\partial m}.$$
 (5.2)

By taking the derivative of Eq. (5.1) with respect to m we get $1 = 2P(h_c)\partial h_c/\partial m$. Using this to replace $\partial h_c/\partial m$ in Eq. (5.2) and setting Eq. (5.2) to zero we get

$$0 = -Jm + \frac{2h_cP(h_c)}{2P(h_c)}$$
$$h_c = Jm$$

and Eq. (5.1) becomes

$$m = 2 \int_0^{Jm} P(h)dh. \tag{5.3}$$

Eq. (5.3) is the ground state mean field equation. Note that m=0 is always a solution as expected.

To determine if the solutions to Eq. (5.3) are minima or maxima one needs the second derivative of the energy with respect to m. If the second derivative at m is greater than

zero, m is a minimum, if it is less, m is a maximum.

$$\frac{\partial^2 (E_x + E_h)}{\partial m^2} = -J + \frac{\partial h_c}{\partial m} = -J + \frac{1}{2P(h_c)}$$

If $J > 1/2P(h_c)$, m is a minimum and if $J < 1/2P(h_c)$, m is a maximum. In addition to this comparison it is also necessary to compare the energy for the cases m = 0 and m = 1 to that of the non-trivial solution m_s .

Now let's do the calculation for four particular distributions of random fields:

$$\rho_1(h) = \frac{1}{2}\delta(|h| - H)$$

(see 5.1.1),

$$\rho_2(h) = \frac{1}{\sqrt{\pi}H} \exp(-\frac{h^2}{H^2})$$

(see 5.1.2),

$$\rho_3(h) = \frac{y+1}{2Hy} \left(1 + \left(\frac{|h|}{H} \right)^y \right) \tag{5.4}$$

and

$$\rho_4(h) = \frac{y+1}{2H} \left(\frac{|h|}{H}\right)^y - 1 < y < \infty \tag{5.5}$$

(see 5.1.3). The first two cases were considered by Aharony and the last two illustrate the nonuniversality of the second order phase transition.

5.1.1 Bimodal distribution

A bimodal distribution is an extreme case in the sense that there is only one possible magnitude of the random fields. Only the direction of the fields can differ between two neigh-

boring sites. For this distribution Eq. (5.3) becomes

$$m = \int_0^{Jm} \delta(|h| - H) dh,$$

which is only non-zero if Jm > H. It therefore reduces to

$$m = \left\{ \begin{array}{ll} 1 & J > H \\ 0 & \end{array} \right.,$$

which clearly marks it as a first order transition with the critical point at H = J.

5.1.2 Gaussian distribution

A Gaussian distribution is quite different from the bimodal one. Most of its weight is near the origin but there is also an exponentially small probability for very large fields. This changes the behavior of the transition significantly. A large field, h > cJ where c is the connectivity of the site, will always be able to force the local spin in alignment. On the other hand the cooperation of many small fields is necessary to flip a spin cluster of the order of the system size.

The ground state mean field equation is

$$m = 2 \int_0^{Jm} \frac{1}{\sqrt{\pi H}} \exp(-\frac{h^2}{H^2}) dh, \tag{5.6}$$

which can be rewritten in terms of the error function $m={\rm erf}({\rm Jm/H})$. Unfortunately, except for the solution m=0, this equation can only be solved numerically. Nevertheless this solution is important since it becomes the *minimum* solution when J>1/2P(0) or $H/J>2/\sqrt{\pi}$.

Next expand Eq. (5.6) for small m

$$\delta m = \frac{2J\delta m}{H\sqrt{\pi}} - \frac{2J^3\delta m^3}{3H^3\sqrt{\pi}} + O(\delta m^4),$$

which again has the obvious solution of $\delta m = 0$.

$$1 = \frac{2J}{H\sqrt{\pi}} - \frac{2J^3 m^2}{3H^3\sqrt{\pi}}$$

$$\delta m^2 = \left(\frac{2J}{H\sqrt{\pi}} - 1\right) \frac{3H^3\sqrt{\pi}}{2J^3}$$

$$\delta m = \left(\frac{3\sqrt{\pi}}{2}\right)^{1/2} \frac{H}{J} \left(\left(\frac{H}{J}\right)_c - \frac{H}{J}\right)^{1/2}$$

where $(H/J)_c=2/\sqrt{\pi}$ as expected and $m\sim \Delta (H/J)^{1/2}$.

5.1.3 Polynomial distributions

To test universality further, we use the distributions ρ_3 and ρ_4 , that are defined on the interval $-H \leq h \leq H$. These distributions have an additional tunable parameter. The exponent y determines the shape of the distribution. For small values of y, ρ_3 is sharply peaked at the origin, whereas for $y \gg 1$ it approaches a uniform deviate (see Fig. 5.1).

The solution of Eq. (5.3) can be found for a general y

$$m = 2 \int_0^{Jm} \frac{y+1}{2Hy} \left(1 - \left(\frac{|h|}{H} \right)^y \right) dh.$$

Since the upper and lower bound of the integral are positive it is not necessary to take the

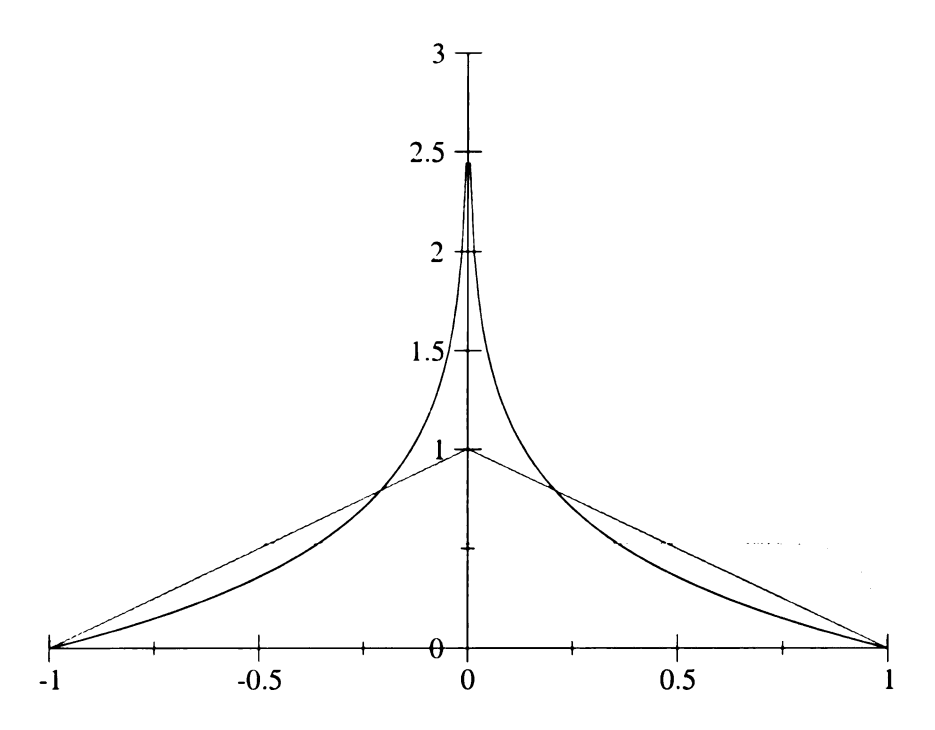


Figure 5.1: Tunable random distribution. $\rho_3(h) = \frac{y+1}{2Hy} \left(1 - \left(\frac{|h|}{H}\right)^y\right)$ for y=1/20 (top), 1 (middle), and 20 (bottom).

absolute value of h and it is easy to do the integration explicitly

$$m = \frac{(y+1)}{Hy} \left[h - \frac{H}{y+1} \left(\frac{h}{H} \right)^{y+1} \right]_0^{Jm}$$
$$= \frac{(y+1)}{Hy} \left(Jm - \frac{H}{y+1} \left(\frac{Jm}{H} \right)^{y+1} \right).$$

Solving the above equation gives m = 0 and

$$1 = \frac{(y+1)}{Hy} \left(J - \frac{J}{y+1} \left(\frac{Jm}{H} \right)^y \right)$$
$$\left(\frac{y+1}{y} - \frac{H}{J} \right) \frac{J}{H} = \frac{1}{y} \left(\frac{J}{H} \right)^{y+1} m^y$$
$$m = y^{1/y} \left(\left(\frac{H}{J} \right)_c - \frac{H}{J} \right)^{1/y} \frac{H}{J}$$

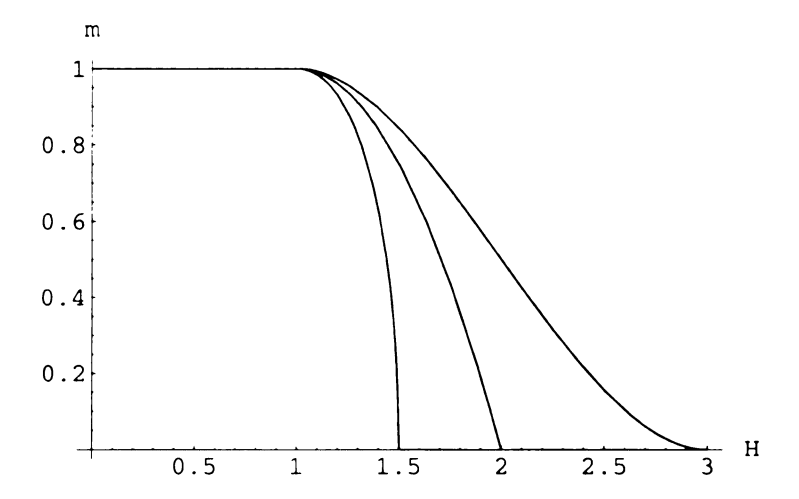


Figure 5.2: Magnetization for different distributions of random fields. This shows the magnetization for $\rho_3(h) = \frac{y+1}{2Hy} \left(1 - \left(\frac{|h|}{H}\right)^y\right)$ with y=2 (left), 1 (middle) and 1/2 (right).

where $(H/J)_c=(y+1)/y$. The magnetization decays like $m\sim \Delta(H/J)^{1/y}$ near the critical point.

This is quite remarkable since it shows that the exponent depends *explicitly* on the exact shape of the distribution and is therefore *not* universal.

Now I briefly consider the distribution $\rho_4(h)$ given in Eq. (5.5). For y > 0 this distribution is bimodal. In this case, it is easy to confirm the conclusion of Aharony that the transition is first order. However the cases -1 < y < 0 are more interesting. In these cases the disorder is dominated by small random fields, as the distribution is singular at the origin (though it is integrable). It is easy to carry out the mean-field calculation (5.3) with the result,

$$m_{eq} = \left(\frac{H}{J}\right)^{1+1/y} \qquad H > J \tag{5.7}$$

By comparing the energies of E(m=0), E(m=1), and $E(m_{eq})$, I find that for H < J the ground state is fully magnetized, while for H > J the ground state has magnetization (5.7). The interesting feature of the result (5.7) is that there is no phase transition at finite H in this system, and the system always has a finite magnetization. The disorder distribution

(5.5) thus destroys the ground state phase transition, due to the large number of small random fields.

5.1.4 Finite temperature

How does temperature influence the phase transition? If there is a zero-temperature fixed point the nonuniversal behavior described above should also be observable at finite temperature. From 2.2.1 we know that the mean field equation for the Ising model with an external field is $m = \tanh(m/T + H/T)$ (cf. Eq. (2.21)). For the RFIM the external field is not uniform. To take the distribution of random fields into account, multiply the right hand side of Eq. (2.21) by $\rho(h)$ and integrate over h. The mean field equation becomes

$$m = \int_{-\infty}^{\infty} dh \rho(h) \tanh(m/T + h/T).$$

Assuming $\rho(h)$ is symmetric this can be rewritten as

$$m = \tanh(m/T) \int_0^\infty dh \frac{\rho(h)}{1 + \cosh(2h/T)/\cosh(2m/T)}.$$
 (5.8)

There are two regimes $m/T\gg 1$ and $m/T\ll 1$. At zero temperature only the first regime is applicable. But at any finite temperature the second regime is applicable close to the critical point.

If $m/T \gg 1$, $\tanh(m/T) \to 1$ and $\cosh(2h/T)/\cosh(2m/T) \to \exp(2(h-m)/T)$, which yields,

$$m = 2 \int_0^\infty \frac{\rho(h)dh}{1 + \exp(2(h-m)/T)} \quad m/T \to \infty.$$

Note that this equation looks like a Sommerfeld integral for a free Fermi gas with the Fermi Energy given by $\epsilon_f = m$. The leading order term for the low temperature expansion is thus the integral of $\rho(h)$ from zero to m. This is the same as Eq. (5.3).

If $m/T \ll 1$, then $\cosh(2m/T) \to 1$ and Eq. (5.8) reduces to the mean field equation for the thermal transition, albeit with an additional factor of two in the argument and a renormalized coefficient in front.

$$m = 2I(H, T) \tanh(2m/T)$$
 $m/T \rightarrow 0$

where

$$I(H,T) = \int_0^\infty dh \frac{\rho(h)}{1 + \cosh(h/T)}.$$

Therefore at any finite temperature, provided that $m/T \ll 1$, an expansion to third order shows that the magnetization approaches zero with exponent $\beta = 1/2$.

Thus for finite temperature the universal mean field exponent $\beta = 1/2$ is recovered. This is surprising, since it was assumed previously that the RFIM is dominated by a zero temperature fixed point. At least for the infinite range model this is not true.

5.2 Cayley tree

Motivated by the results from the previous sections, we have analyzed the zero temperature RFIM on a Cayley tree, or *Bethe* lattice, for a variety of disorder distributions. We find that the *Bethe lattice is universal*, provided the transition is second order, even in the limit of large coordination. This is surprising since in this limit the Bethe lattice usually approaches the mean field limit.

The Hamiltonian of the random-field Ising model is

$$\mathcal{H} = -\sum_{ij} J_{ij} S_i S_j - \sum_{i} (B + h_i) S_i, \tag{5.9}$$

where the exchange is ferromagnetic $(J_{ij}>0)$ and the fields h_i are random and uncorre-

lated. The random fields are drawn from a specified distribution $\rho(h)$.

We determine whether the nonuniversal results found above for the mean field theory extend to the ground state of the RFIM on a Cayley tree. The coordination number of a tree is taken to be z, while the probability that a spin is up is P_+ and the probability that a spin is down is P_- . The probability that a spin is up at level l can be written in terms of the probabilities of the level that is one lower down in the tree. This leads to a recurrence relation similar to P for percolation discussed in 2.4. This yields [14, 10]

$$P_{+}(l) = \sum_{g=0}^{\alpha} \begin{pmatrix} \alpha \\ g \end{pmatrix} P_{+}^{g}(l-1)P_{-}^{\alpha-g}(l-1)a_{+}(\alpha,g)$$
 (5.10)

where $a_+(\alpha, g)$ is the probability that the local effective field is positive when g neighbors are up. The local effective field combines the local random field with the spin-spin interaction of the neighbors. The idea is similar to the molecular field in the mean field Ising model (cf. 2.2.1). If we know the distribution $\rho(h_i)$, we can compute $a_+(\alpha, g)$. Analyzing the equilibrium behavior, we have

$$a_{+}^{eq}(\alpha, g) = \int_{(\alpha - 2g)J - H}^{\infty} \rho(h)dh. \tag{5.11}$$

By direct iteration of the recurrence relation (5.10) we show that a stable steady state solution, $x = P_+^* = 1 - P_-^*$, exists (cf. 2.4.1)

$$x = \sum_{g=0}^{\alpha} \begin{pmatrix} \alpha \\ g \end{pmatrix} x^g (1-x)^{\alpha-g} a_+(\alpha, g)$$
 (5.12)

It is easy to solve equation (5.12) for small values of α . For $\alpha=1,\ 2$ Cayley trees have no ordered state for any finite H, for the disorder distribution (5.4). But for $\alpha=3$ a ferromagnetic state does exist for a range of disorder. As we see from Eq. (5.10), the $\alpha=3$

case leads to a polynomial of order 3,

$$x = (1-x)^3 a_+(3,0) + 3x(1-x)^2 a_+(3,1) + 3x^2(1-x)a_+(3,2) + x^3 a_+(3,3),$$

which can be simplified to,

$$\frac{m}{4}[m^2(1-3b+a)-1+3a+3b]=0$$
(5.13)

were $m=2(P_+^*-1/2)$, $a=a_+^{\rm eq}(3,0)=1-a_+^{\rm eq}(3,3)$ and $b=a_+^{\rm eq}(3,1)=1-a_+^{\rm eq}(3,2)$. Eq. (5.13) has the following solutions:

$$m = 0;$$
 and $\pm \left(\frac{3a + 3b - 1}{3b - 1 - a}\right)^{1/2}$. (5.14)

These solutions apply for any disorder distribution. For the distribution $\rho_3(h)$, performing the integrals yields,

$$m = \left[\frac{4y - 12(y+1)\overline{J} + 3(3^{y+1} + 1)\overline{J}^{y+1}}{3(1 - 3^y)\overline{J}^{y+1}} \right]^{1/2}$$
 (5.15)

We can now expand the magnetization around the critical point, J_c , $\overline{J}=\overline{J}_c-\epsilon$. We find,

$$m \sim \left[(-12(y+1) + 3 \begin{pmatrix} y+1 \\ y \end{pmatrix} (1+3^{y+1}) \overline{J}^y) \epsilon \right]^{1/2}$$
 (5.16)

Thus $m \sim \epsilon^{1/2}$ for any y, so that $\beta=1/2$ is universal. Since the non-equilibrium behavior on trees is related to that of the equilibrium behavior by a simple shift, this universality extends to the hysteresis and avalanche exponents. It is easy to confirm numerically that the behavior extends to large values of the branch coordination number α . Moreover by doing an expansion of (5.10) using $P_+=1/2+m$, it is possible to show analytically that

only the first and third order terms in m exist (see Appendix A), regardless of the value of y in the disorder distribution (5.4). This confirms that for this distribution, the behavior is universal for all coordination numbers.

For the distribution $\rho_2(h)$ and $\alpha = 3$ we get from Eq. (5.14)

$$m = \left[\frac{4 - 3(3^{y+1} + 1)\overline{J}^{y+1}}{3(3^{y} - 1)\overline{J}^{y+1}} \right]^{1/2}.$$
 (5.17)

Just like we have done before we can expand m around the critical point, $\overline{J} = \overline{J_c} - \epsilon$:

$$m \sim \left[\left(\begin{array}{c} y+1 \\ y \end{array} \right) (3^{y+1}+1)) \overline{J_c}^y \epsilon \right]^{1/2}.$$

Thus for ρ_2 , $\beta = 1/2$ is a universal exponent, too.

5.3 Numerical ground state calculations of the RFIM

To see which of the two models is closer to the RFIM in 3D I use the mapping of the RFIM to the maximum flow problem (see 4.2.2). I find the ground states for cubic systems with periodic boundary conditions. Gaussian and bimodal distribution have been previously studied [13, 39, 46]. To test universality I use the distribution ρ_4 with y=0.5 and y=-0.5. The positive exponent leads to a bimodal distribution for ρ_4 and in the mean field limit gives a first order phase transition, whereas for y=0.5 the magnetization decays as 1/H.

Determining the critical field has been a challenge for RFIM studies from the beginning. I will look at several quantities to extract both the critical field as well as the exponents: a) the differential of the magnetization, b) the standard deviation of the magnetization $\sigma(m)$, c) the execution time, and d) the critical field. For a, b, and c I study the peak position and peak height. For d I only look at the change in the value for different system sizes. All

Name	Description	RFIMBench
zufall	Dual Xeon 550MHz, 2GB RAM	1
pannonia	AMD Athlon 1GHz, 512MB RAM	1.12
cojocaru, fay, musolffc	Pentium 4 1.6GHz, 512MB RAM	1.56

Table 5.1: Benchmark results for the random-field Ising model (see text).

quantities should show a power law behavior with respect to the system size of the form

$$\max(x) \sim L^{-a/\nu} \tag{5.18}$$

$$\sigma(x) \sim L^{-b/\nu} \tag{5.19}$$

$$H_c \sim H_c^{\infty} + aL^{-c/\nu} \tag{5.20}$$

where ν is the correlation length exponent. In particular for $\sigma(m)$,

$$\sigma(m) \sim L^{-2\beta/\nu}$$
.

To compare results from different computers I ran a 50^3 sample with $H \in [2,5]$ and $\delta H = 0.125$ using the same realization of random fields on all systems. I defined the result on zufall as 1. Higher benchmark values indicate a faster computer. For details see Table 5.1.

I find the maximum time for each run and average over all realizations for a given system size and distribution exponent. I plot both the average and the standard deviation vs. L on a log-log scale (see Fig. 5.3).

The standard deviation of the magnetization $\sigma(m)$ vs. L (see Fig. 5.4) is very flat. This leads to a value of $2\beta/\nu \approx 0$ and therefore $\beta \approx 0$. This agrees with previous results for both Gaussian and bimodal distributions in 3D but not with the results from the infinite-range calculation.

I used the locations of the maximum of the calculation time, the maximum of $\sigma(m)$,

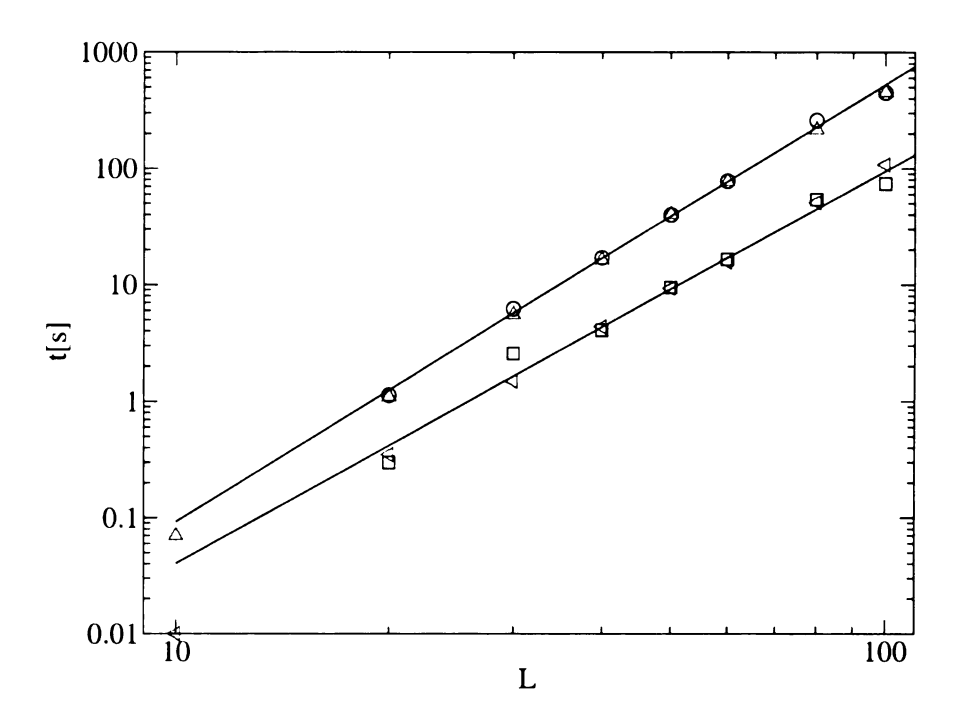


Figure 5.3: Maximum execution time vs. L. The circles and up-triangles are the maximum times obtained for y=0.5 and y=-0.5 respectively. The squares and the left-triangles are the respective standard deviations. Each point has been averaged over all available realizations. The solid lines are least squares fits to power laws, $y \sim x^a$ with a=3.75 for the upper curve and a=3.37 for the bottom one.

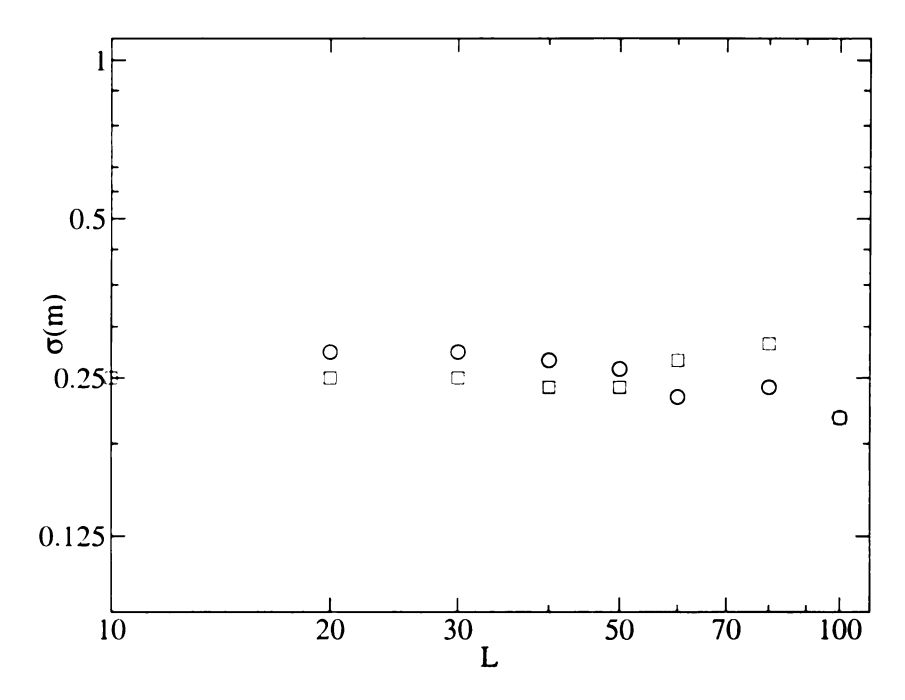


Figure 5.4: Maximum standard deviation of the magnetization. The circles are the data for y = 0.5, the squares are for y = -0.5. Both are essentially flat.

and the maximum of the differential of the magnetization to determine the critical field H_c^L . The results are in good agreement with each other (see Fig. 5.5). The large number of small fields in ρ_4 with y=-0.5 leads to a larger critical field value than y=0.5. The approach to the infinite volume limit leads to different values of ν .

I also used the finite size scaling relation

$$M = ML^{\beta/\nu}\widetilde{M}\left((H - H_c^{\infty}) L^{1/\nu} \right)$$

to determine ν and β . I achieved the best collapse for $H_c^\infty=3.30(5)$, $\nu=2.00(5)$, and $\beta=0.00(1)$ for y=0.5 (see Fig. 5.6) and $H_c^\infty=5.00(5)$, $\nu=1.50(5)$, and $\beta=0.00(1)$ for y=-0.5 (see Fig. 5.7). The errors in H_c^∞ , ν , and β are estimated from the quality of the collapse.

The timing exponent is universal for the two distributions. As in previously published

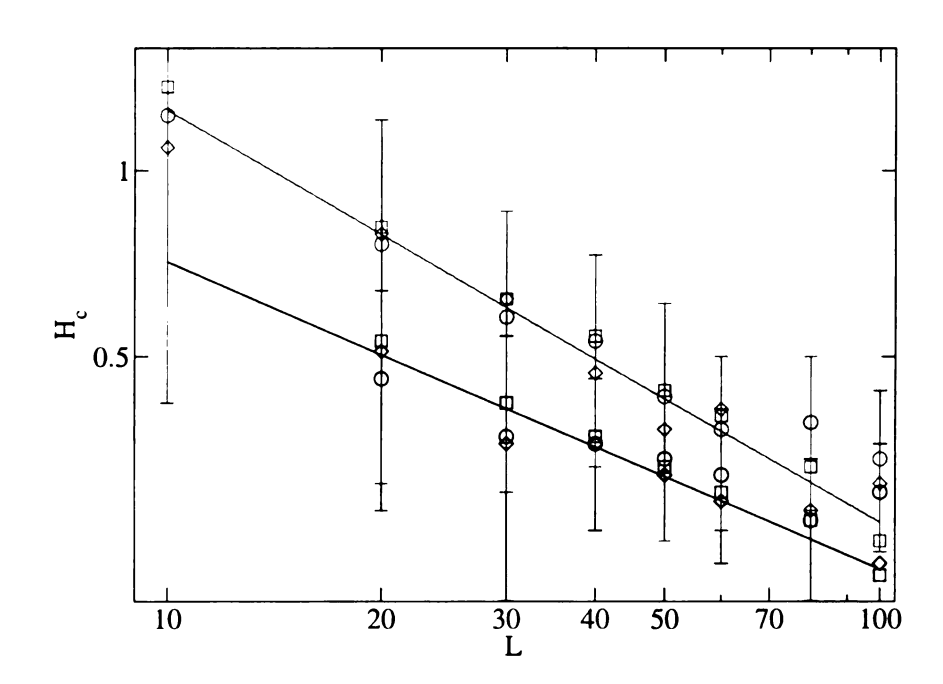


Figure 5.5: Finite size scaling of the critical width of the distribution. The critical width of the distribution H_c^L is determined in three independent ways: The maximum of the execution time (circles), the maximum magnetization jump (squares), and the maximum of the standard deviation of the magnetization (diamonds). All three values are in good agreement. The plot shows $H_c^L - H_c^\infty$. The solid lines are fits of the form $(H_c^L - H_c^\infty)^{-\delta}$ with $\delta = 1/\nu$. $\delta = 0.5$ for y = 0.5 and $\delta = 0.66$ for y = -0.5. The error bars are given for the values determined by the maximum execution time.

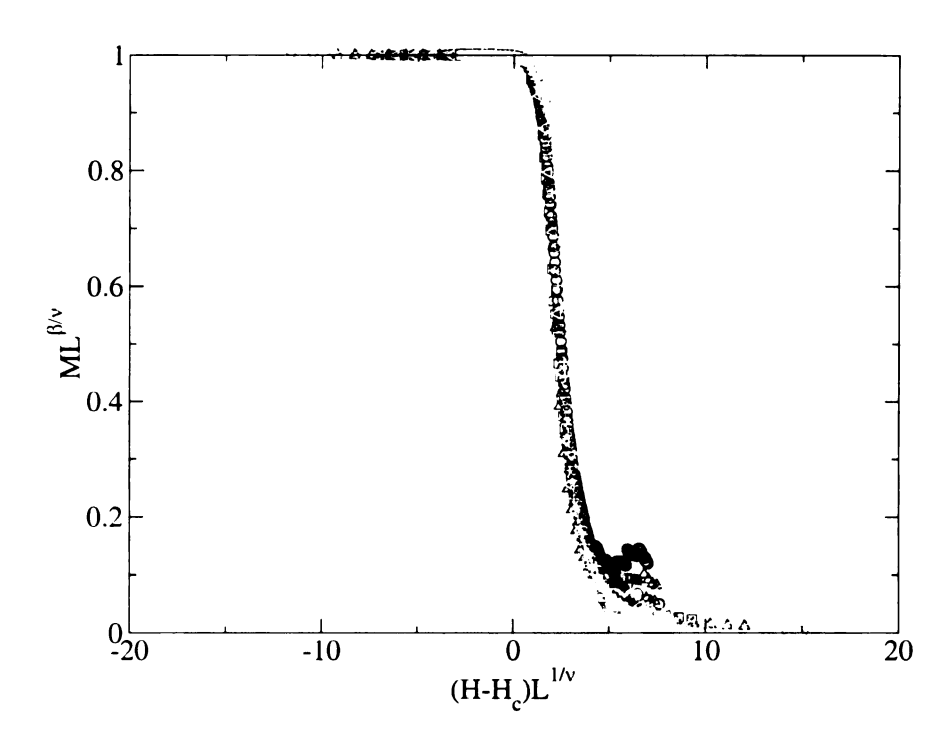


Figure 5.6: Scaling plot for the magnitude of the magnetization for ρ_4 with y=0.5 and L=20,30,40,60,80,100. For this fit I used $H_c^\infty=3.3$, $\nu=2.0$, and $\beta=0.0$.

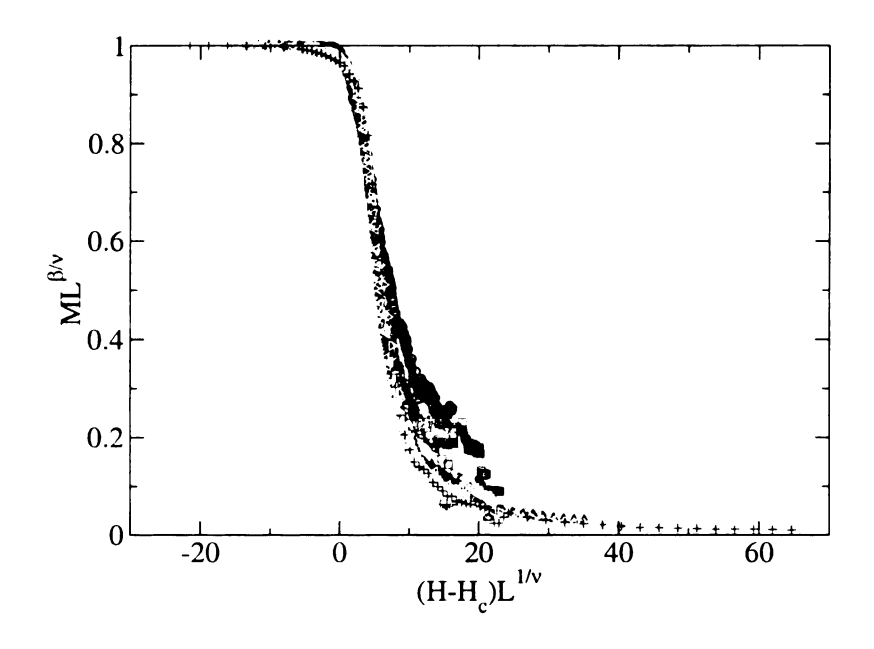


Figure 5.7: Scaling plot for the magnitude of the magnetization for ρ_4 with y=-0.5 and L=10,20,30,40,60,80,100. For this fit I used $H_c^\infty=5.0,\,\nu=1.5,$ and $\beta=0.0.$

work [20] the scaling is consistent with $\beta=0$. This is in contradiction to the infinite-range model prediction. The correlation length exponent on the other hand is not universal nor does it agree with the exponents previously obtained for Gaussian and bimodal distribution where $\nu=1.2$ and $\nu=1.67$ respectively [13, 20].

In this chapter I presented the behavior of the RFIM with infinite-range interactions. I showed that the behavior of the magnetization near the critical point depends explicitly on the distribution of random fields for T=0K. This nonuniversality does not extend to finite temperature. The behavior of the infinite-range random-field model is therefore *not* dominated by a zero-temperature fixed point.

In summary, I find that the stretched exponential disorder distribution leads to a nonuniversal order parameter exponent in the RFIM mean-field theory at T=0K. In contrast the Cayley tree does not show this nonuniversality. The order parameter exponent of the RFIM in 3D with short range interactions is so small that the issue of universality in β seems a moot point there. The behavior in dimensions higher than three, or for longer range interactions in three dimensions, however, should be interesting. In addition, even for short range interactions in three dimensions, I see nonuniversality in the finite size scaling behavior. This is compatible with previously published results for bimodal and Gaussian distributions [13]. The physical origin of this nonuniversality is unclear at present.

Chapter 6

Interfaces in Disordered Systems

Damascus blades made in the 16th and 17th century are among the best blades known to man. Their strength and beauty made them popular items in trade and warfare and more recently as collectors and museum pieces. The art of making Damascus blades had been lost for centuries and has only recently been rediscovered [55, 54]. Materials researchers studying these blades find themselves faced with other obstacles besides analyzing the composition and structure of the metal. The valuable blade has to be destroyed to analyze it. But some blades have been donated for analysis. They have helped rediscover the making of Damascus blades and furthered our understanding of what makes them so tough. The steel used to forge a Damascus blade is imported from India and called wootz. The composition and structure of the impurities in wootz steel are essential for forging as well as the blade's final properties. During the cooling of the blade the iron freezes in the shape of inverted pine trees. The impurities segregate out of the solid iron and form bands. These impurity bands form the seeds for the growth of iron carbide (Fe_3C) particles during subsequent heating and cooling cycles. The iron carbide bands increase the average internal grain binding energy within the blade, while embedding the bands in the softer steel effectively increases the adhesion energy between grains. This combination leads to a high minimum fracture energy and provides a plausible explanation for the strength and toughness of Damascus blades.

Low energy surfaces play a critical role in growth, material processing, and controlling material properties [59, 50]. The morphology and energy of crystal surfaces have been heavily studied, as have misoriented interfaces between two single crystals. In this study, Phil Duxbury and I consider the lowest energy surface through a polycrystalline aggregate. This is a multiscale problem. Atomistic simulations can provide the grain boundary energies, while a higher level calculation is required to find the energy of separation of the polycrystal. We develop a graph representation of the polycrystal. Each bond in the graph has an assigned energy that depends on whether it is in the interior of a grain or on a grain boundary.

6.1 Models and methods

The favorite model of a solid in condensed matter physics is a regular, infinite crystal. Many metals and other materials form large crystals that can be described by a repeated unit cell. Most real world materials, however, are not *single* crystalline but consist of crystal grains of different sizes and orientations. Grain sizes play an important role for their properties such as stress and strain resistance, critical currents in superconductors, or the roughness of the fracture surface.

Using the Potts model of grain growth [24] I generated the model grain structures I used to test the scaling predictions. The grain structures produced by this model have been shown to reproduce the grains size statistics of metals and ceramics accurately [47, 5].

The Potts model is a generalization of the Ising model that allows q distinct spin states.

The Hamiltonian is

$$\mathcal{H} = -J \sum_{ij} \delta(s_i, s_j) \tag{6.1}$$

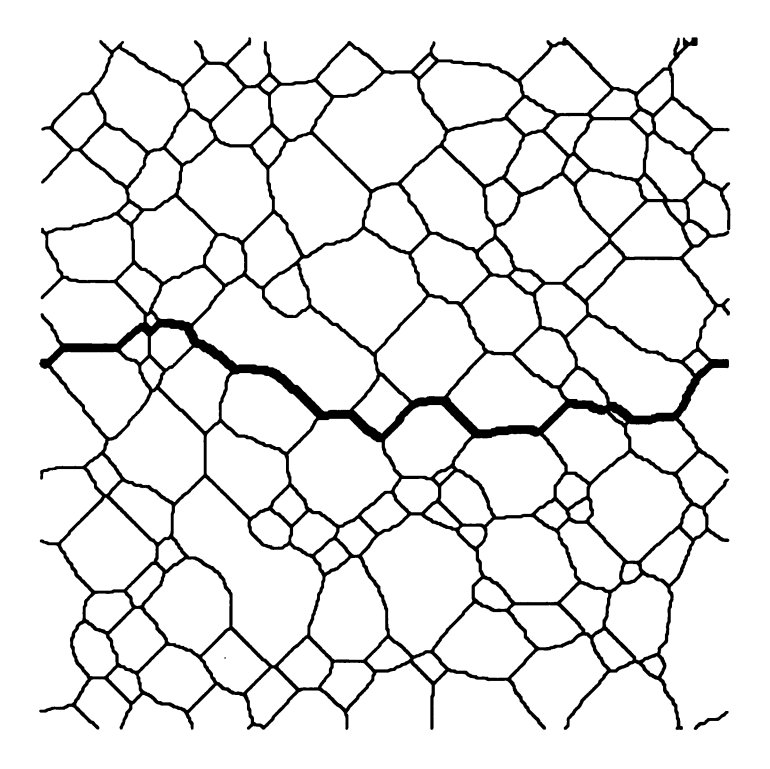


Figure 6.1: 2D Grain Structure. The thick line through the grain structure indicates the minimum energy surface for weak adhesion.

where the interaction is not necessarily limited to nearest neighbors. In fact I used a square lattice with nearest and next-nearest neighbor interactions to produce the grain structures in this work. δ is the Kronecker δ . It is 1 if s_i and s_j are equal, and 0 otherwise.

The starting configuration is created by assigning random numbers between 1 and q to each site. Then the algorithm picks sites randomly, changes the spin and checks if the overall energy is lower than before. If the total energy is lower, the change is accepted; otherwise it is rejected. This is a T=0K Monte Carlo method. The actual program uses an improved algorithm. Instead of picking a new *random* value for the spin between 1 and q it chooses among the values of the neighboring spins. Once the grains have grown enough, the algorithm takes advantage of the fact that changes can only occur at the grain boundaries [22] and not in the interior of a grain.

We have two energies in our model: ϵ_g is the internal binding energy of the grain and ϵ_i is the adhesion energy between grains. The relevant energy scale in our calculations is

 $\epsilon = \epsilon_i/\epsilon_g$. To find the minimum energy interface we map the grain structure to a graph. The spins are the nodes and we assign a capacity to each edge. If an edge connects two nodes with equal spins its capacity is ϵ_g , if the spins differ it is ϵ_i . The resulting graph is equivalent to a random-bond Ising model (see 3.1) and the minimum energy interface is the minimum cut (see 4.2.1).

The connection between domain walls in Ising magnets and the minimum cut/maximum flow problem has led to improved precision in the calculation of the energy, energy fluctuations, and roughness of these interfaces [38, 2]. Here I extend the scaling theories for domain walls in random Ising magnets and their supporting numerical analysis to graphs that represent a polycrystalline microstructure. I show that the roughening transition of domain walls corresponds to the transition from cleavage to intergranular interfaces in polycrystalline materials. Fig. 6.1 and Fig. 6.2 give examples of minimum energy surfaces in the 2D grain structures I used.

One application of the analysis is the study of fracture surfaces [8]. The experimental evidence suggests that fracture surfaces have a roughness exponent in the range $0.5 \le \zeta \le 0.85$. It has been suggested that at short length scales, the "quasistatic" exponent should apply [8, 41]. Raisanen et al. have shown that for mode III failure (or scalar quasistatic failure) this exponent is close to 0.42 [41] in three dimensions. Many of the experiments, however, are carried out in polycrystalline materials, so it is important to test the effect of polycrystalline morphology on the quasistatic exponents. For the case of weak grain boundaries in two dimensional systems, the intergranular interface problem was recently simulated [23] and it was found that the ball and spring model [44, 7] produces surfaces that have similar properties to the minimum energy surface. Allowing grain boundaries to have a range of bonding strengths allows the possibility of a transition from cleavage to intergranular interfaces. To describe the large length scale properties of these minimal energy surfaces, I develop a scaling theory based on those for domain walls [26, 17] and

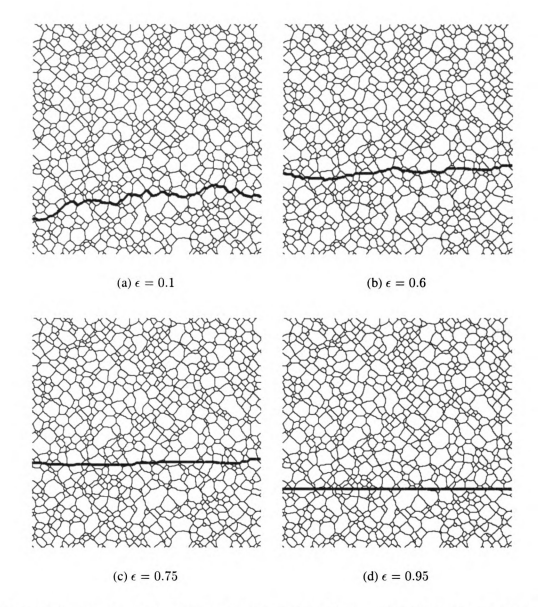


Figure 6.2: Image of a grain structure with $g\simeq 16$ and L=500. The 4 frames show the interface for different adhesion strength.

for periodic elastic media [9, 15, 45].

6.2 Weak adhesion limit $\epsilon \to 0$

In the limit of weak grain boundary adhesion ($\epsilon \to 0$), the minimal energy surface through the polycrystalline material follows the grain boundaries. The scaling laws for the interface energy and the interface roughness are found by extending the theory for random manifolds. An example of a random manifold is a minimal energy surface through a hypercubic Ising magnet where the exchange constants are all ferromagnetic, but random. There is a well developed theory for this problem [26, 17] and the scaling predictions are: The energy of the minimum energy surface E scales as $E=a_1L^{d-1}+a_2L^{\theta}$, where θ is a universal exponent with $\theta=1/3$ in two dimensions and $\theta=0.82(2)$ in three dimensions [38, 2]. The surface roughness is $w=\sqrt{\langle h^2\rangle-\langle h\rangle^2}=b_1L^{\zeta}$ where $\zeta=2/3$ in two and $\zeta=0.41(1)$ in three dimensions. ζ and θ are universal exponents that do not depend on the details of the disorder or lattice structure. A quantity that is not usually treated, but that is of interest in many problems, is the number of bonds on the minimal energy surface N, which scales as $N=c_1L^{d-1}+c_2L^{\theta}$.

Let's extend the above scaling laws for random manifolds to the case of interest here. The average grain size acts like the lattice constant so that L/g is the effective system size. The scaling laws for the energy of the minimal energy surface lying along the grain boundaries is given by

$$E = g^{d-1} \left[a_1 \left(\frac{L}{g} \right)^{d-1} + a_2 \left(\frac{L}{g} \right)^{\theta} \right]. \tag{6.2}$$

If we ignore the correction term and rescale by L^{d-1} the energy is

$$\frac{E}{L^{d-1}} \approx a_1 \tag{6.3}$$

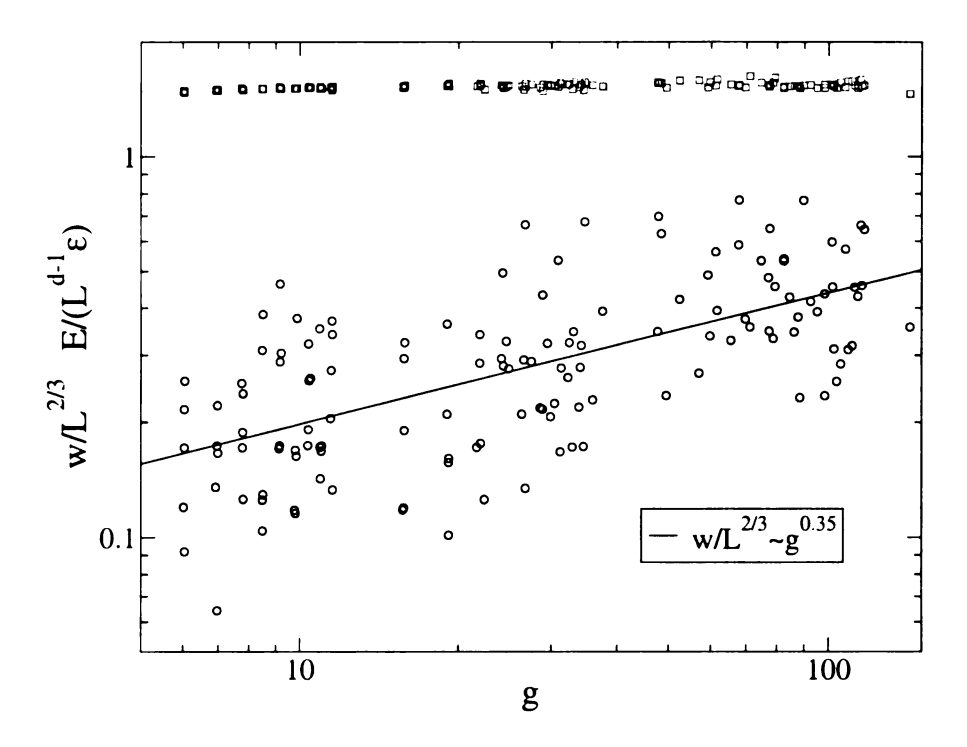


Figure 6.3: Plots of the scaled energy (E/L), squares) and roughness $(w/L^{2/3})$, circles) as a function of the average grain size of polycrystalline materials, in the limit of weak grain boundaries $\epsilon \to 0$. The system sizes are L=500, 1000, 1200, and 2000. Each point is a single data point. The data are well described by the scaling prediction (6.3) of an interface energy which is asymptotically independent of the grain size E = const and of a roughness, which scales as $w \sim g^{1/3}$ (see Eq. (6.5)).

as shown by the squares in Fig. 6.3.

The roughness scales as

$$w = b_1 g \left(\frac{L}{g}\right)^{\zeta} \text{ or } \frac{w}{L^{\zeta}} = b_1 g^{1-\zeta}.$$
 (6.4)

In 2D - where ζ is 2/3 - this becomes

$$\frac{w}{L^{2/3}} \approx b_1 g^{1/3} \tag{6.5}$$

In Figure 6.3, we see that both relations (6.3) and (6.5) are in good agreement with the numerical data. The plot shows individual data points. The broad scatter of the roughness

is typical for quenched disordered systems, which self-average very slowly. The width of the scatter decreases, however, with increasing system size.

The energy, in this limit, is proportional to the number of bonds N in the interface

$$E = \epsilon_a \epsilon N \tag{6.6}$$

and N must therefore scale like the energy

$$N = g^{d-1} \left[c_1 \left(\frac{L}{g} \right)^{d-1} + c_2 \left(\frac{L}{g} \right)^{\theta} \right].$$

As we shall see in Section 6.3, the weak adhesion limit applies over quite a broad range of grain boundary energies, with a mixed transgranular and intergranular failure regime setting in at $\epsilon_c \approx 1/2$. This onset is nonuniversal and is expected to depend on the lattice structure. In the simulations described here there is an underlying square lattice. The critical boundary energy can be estimated by considering the conditions under which the interface prefers to cleave a section of the grain containing two atoms. In this case the energy to cleave the two atoms is $2\epsilon_g$, while the energy to follow the grain boundary is $4\epsilon_i$. Balancing these two energies leads to the critical value $\epsilon_c = 1/2$. These sorts of configurations do occur in the grain structure and are necessary to the evolution of the grain morphology. In contrast a single atom "bump" is much less likely.

A surprising feature of the purely intergranular minimal energy surface is that the number of bonds on the interface is very close to N/L=3/2. This means that for every two steps along the cleavage direction the interface takes one step perpendicular to the cleavage direction. It also means that the typical angle of the minimal energy surface $\theta_{typical} = \arctan(1/2) = 26.6^{\circ}$.

6.3 Strong adhesion limit

The strong adhesion limit applies only in the limit $\epsilon \to 1$. Nevertheless understanding this limit sets the stage for the mixed regime, which exists for $1 \le \epsilon \le \epsilon_c$. For the particular case of grain structures on a square lattice $\epsilon_c \sim 1/2$.

In the limit $\epsilon \to 1$, cleavage occurs, i.e., the interface is flat. The roughness and number of bonds are w=0 and $N=L^{d-1}$ respectively. The energy can be expressed as $E=\epsilon_g \left(f_g+\epsilon f_i\right) L^{d-1}$ where f_g is the fraction of the interface within the grains, f_i is the fraction of the interface along grain boundaries, and $f_g+f_i=1$. We can rewrite the energy in terms of f_i ,

$$E = \epsilon_q \left(1 - f_i + \epsilon f_i \right) L^{d-1}. \tag{6.7}$$

As can be seen from Eq. (6.7) the energy is proportional to ϵ as long as f_i is a constant.

Note that f_i is in general *not* zero as even a flat surface must cross some grain boundaries. For $\epsilon \to 0$, $f_i = 1$, since the interface follows the grain boundaries to take advantage of the cheap grain boundary bonds. For $\epsilon = 1$ a simple argument can also be made. The interface has to cross on average L^{d-1}/g^{d-1} grains. The area of the grain boundary of each crossing is proportional to g^{d-2} and the total area of the interface is L^{d-1} . The fraction of the interface along grain boundaries is then

$$f_i = d_1 \frac{g^{d-2} L^{d-1}}{L^{d-1} g^{d-1}} (6.8)$$

$$f_i = d_1 \frac{1}{g}. {(6.9)}$$

where d_1 is a constant that depends on the details of the grain boundary structure, but is independent of the average grain size g.

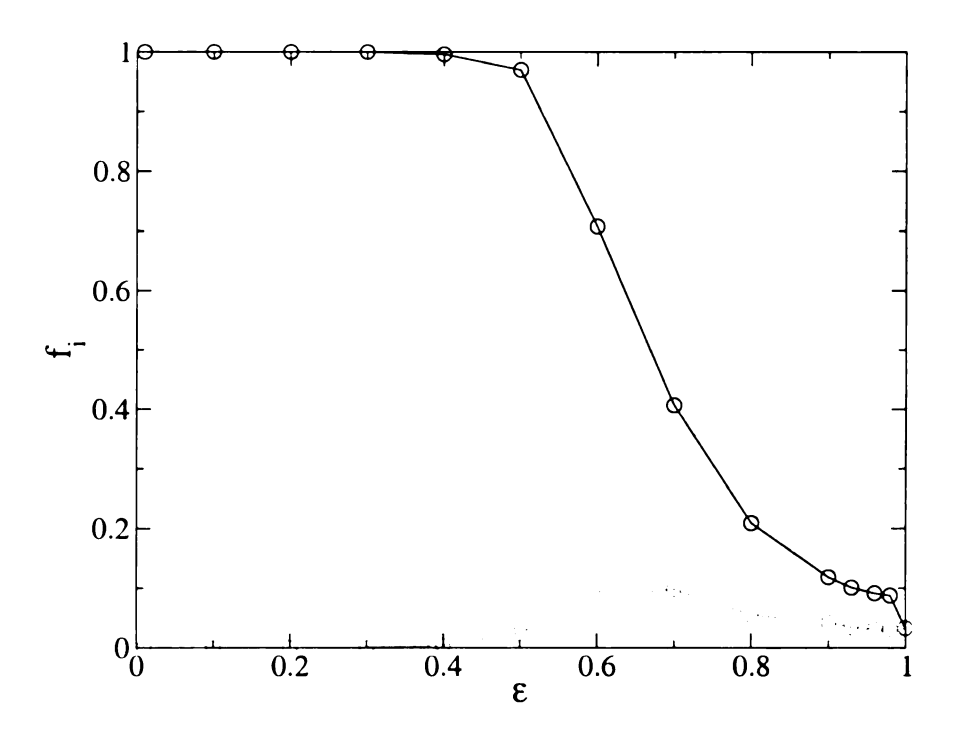


Figure 6.4: Fraction of grain boundary bonds of the interface f_i and its standard deviation vs. ϵ . For this and the following figures each point was averaged over all available system sizes, L=500, 1000, 1200, and 2000, and grain sizes, ranging from $g \simeq 2$ to $g \simeq 350$ depending on the system size. We did not produce grain structures with g/L < 1/3. The top curve shows the average and the bottom curve the standard deviation.

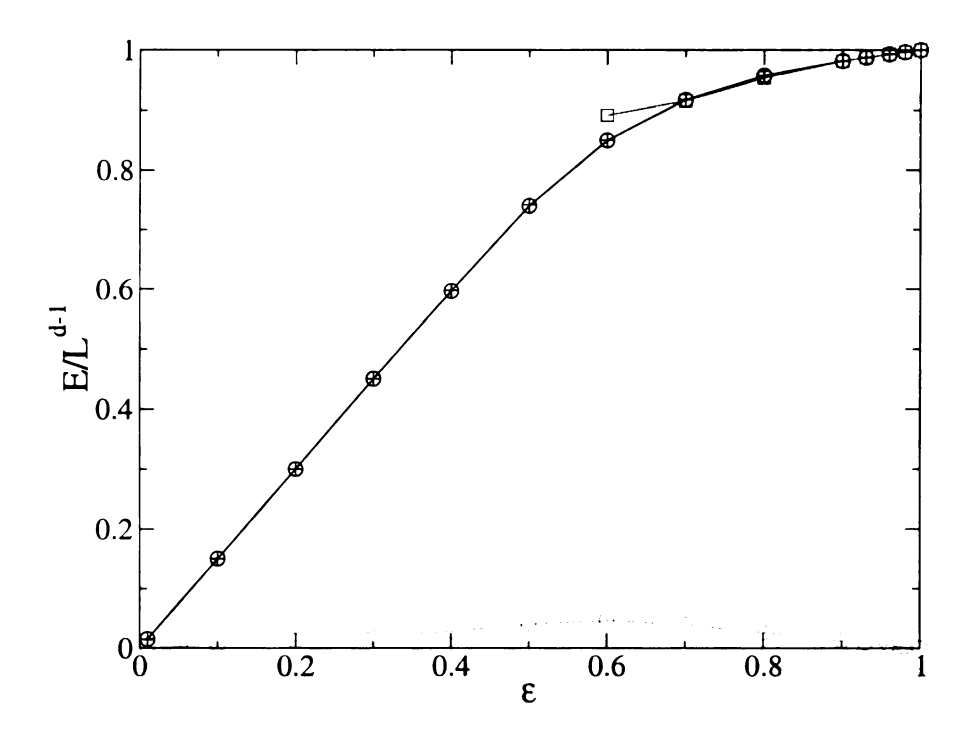


Figure 6.5: Average interface energy (top) and its standard deviation (bottom) vs. ϵ . The plusses are the average energy calculated from Eq. (6.7) verifying the relation. The squares give the fit from Eq. (6.26) and agree well up to $\epsilon \approx 0.7$ (cf. Fig. (6.7)). The bottom curve is the standard deviation of the energy.

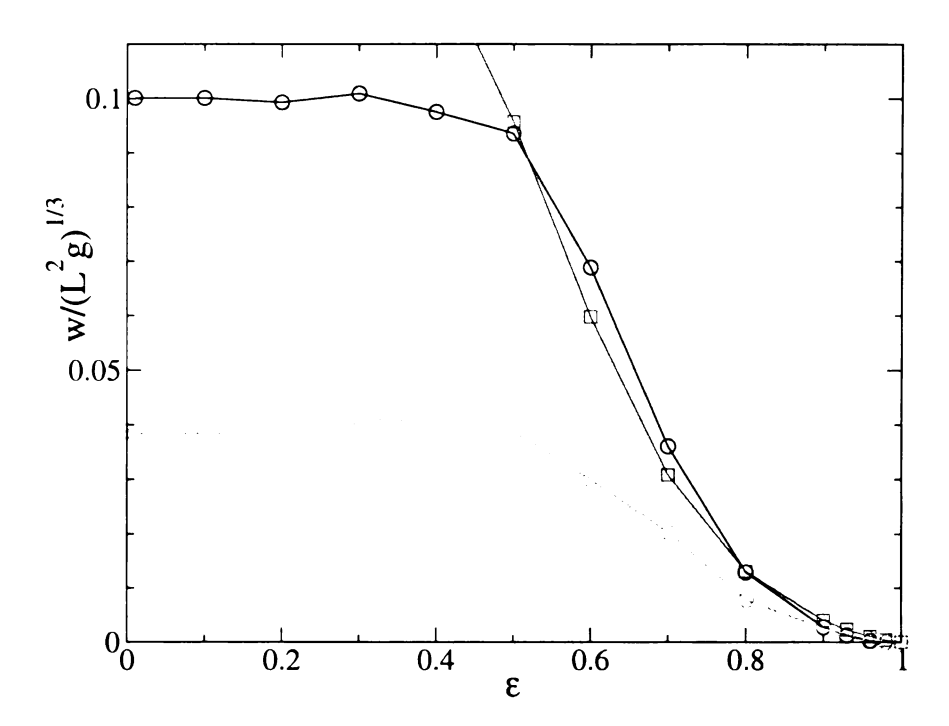


Figure 6.6: Average roughness and its standard deviation vs. ϵ . The circles are the average (top) and standard deviation (bottom) of the data. The squares are the fit using Eq. (6.21).

6.4 Intermediate regime

Numerical results found from analysis of interfaces in polycrystalline materials as a function of the grain boundary bond strength ϵ are presented in Figs. 6.4-6.7. The weak adhesion behavior persists up to energy ratios $\epsilon \sim 1/2$. At higher grain boundary adhesion we enter the mixed regime, where the intragranular fraction of the interface is a sensitive function of the adhesion energy ϵ . From the discussion in the previous section we know that the energy becomes a non-linear function of ϵ only in the intermediate ϵ regime where f_i is varying (see Fig. 6.5). I now present an analytic argument to describe the way in which the crossover from cleavage to intergranular interfaces occurs in the mixed phase.

Our theory for the onset of the mixed regime is based on theories for the roughening of manifolds in periodic elastic media. The key idea originated with Imry and Ma who constructed a theory for the stability of the ferromagnetic phase in the random-field Ising

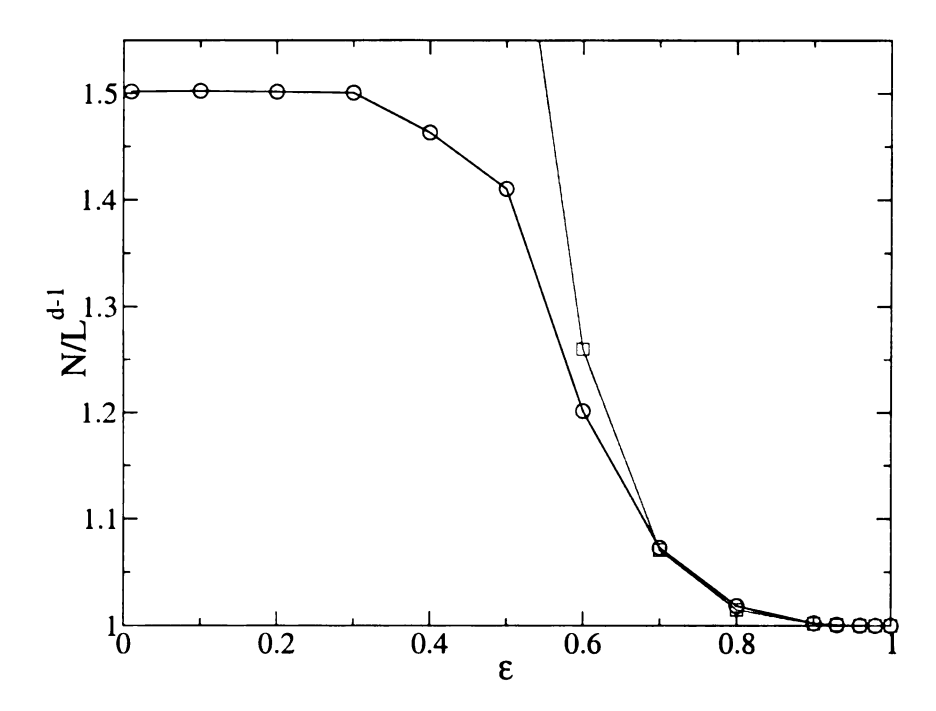


Figure 6.7: Average number of interface bonds and its standard deviation vs. ϵ . The circles are the average of the data. The squares give the fit using Eq. (6.25). The fit agrees well up to $\epsilon \approx 0.7$. The standard deviation is of order 0.05.

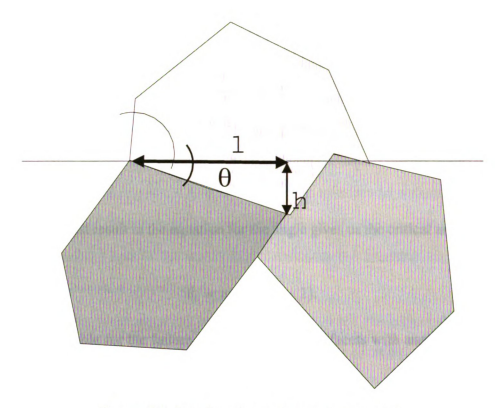


Figure 6.8: Interface through granular material.

model.

We consider in detail faceted grains in two dimensions, as indicated in Fig. 6.8. Whenever the fracture interface encounters a grain boundary it has two choices. It can either go straight through the grain and cleave it or it can follow the grain boundary. The grain boundary makes an angle θ with the cleavage interface. The way along the grain boundary is therefore longer than the cleavage path. The cleavage path has a length l. The length of the facet is l+h due to the underlying square lattice.

The angle $\theta=\arctan(h/l)$. The energy necessary to cleave is $E_c=l\epsilon_g$. The energy to follow the facet is $E_f=\epsilon_i(l+h)$. The fracture interface can only follow the grain boundary

if $E_c \leq E_f$ or equivalently

$$\frac{E_f}{E_c} \geq 1$$

$$\frac{\epsilon(l+h)}{l} \geq 1$$

$$\frac{h}{l} \geq \frac{1}{\epsilon} - 1.$$

Substituting the last result in the equation for the angle gives us the critical angle for a given ϵ ,

$$\theta_c = \arctan(\frac{1}{\epsilon} - 1).$$

It is locally favorable for the failure surface to follow all facets with angles θ smaller than θ_c .

The argument above gives the *local* picture of how the interface roughens. According to this local picture, the local fraction f_L of grain boundaries that lie on a minimal energy surface is given by,

$$f_L = \int_{-\theta_c}^{\theta_c} P(\theta) d\theta \tag{6.10}$$

where $P(\theta)$ is the probability that a grain boundary is at angle θ to the cleavage direction. The average deviation from the cleavage surface is

$$\overline{h} = g \int_0^{\theta_c} \theta \tan(\theta) d\theta.$$

In three dimensions the arguments are more complex. For the arguments below, however, we only need to define a local fraction f_L . A refinement that may be important in some cases, is to include the curvature of the grain boundaries. If curvature is included, the grain boundaries may partially fail. For the grain structures I use here, the grain boundaries are quite faceted.

The argument above describes the local variations in the surface morphology. We seek, however, the *global minimum* energy surface. To find the global minimum we need to consider the energy fluctuations on large length scales. On large length scales, there exist statistically favorable regions where a number of small angle facets are close to each other. It is energetically favorable to include these regions in the minimum energy interface. To include these favorable regions, it is necessary for the interface to wander. The interplay between the desire of the interface to accommodate favorable regions with many low angle facets and the energy cost of the wandering, determines the interface roughness. I now make this energy balance quantitative.

According to the local argument, culminating in Eq. (6.10), the typical number of facets that occur due to local deviations from a cleavage surface is given by

$$N_f = f_L(L/q)^{d-1}. (6.11)$$

The central limit theorem states the typical variation in this quantity is $\delta N_f = N_f^{1/2}$. Such variations can be either positive (unfavorable fluctuations) or negative (favorable fluctuations). In our case, the favorable case corresponds to a clustering of grain boundaries that have low angles to the cleavage direction. There is another factor that must be considered: There are many ways in which a favorable fluctuation on an interface may be selected. That is, the minimal energy fluctuations may occur in many different places in the material. This is an entropy-like factor. The typical number of ways that the set N_f of facets may be selected on a cleavage plane is of order (L/g). To include this factor in estimating the typical largest energy gain, set

$$\frac{L}{q}\exp(-\delta N_f^2/N_f) \approx 1 \tag{6.12}$$

The typical size of the most favorable fluctuation in the number of low angle facets in a

minimal energy surface is then

$$\delta N_{f,max} \approx f_L^{1/2} \left(\frac{L}{g}\right)^{(d-1)/2} \log^{1/2} \left(\frac{L}{g}\right)$$
 (6.13)

The typical energy gain for each favorable facet is $\epsilon_g(1-\epsilon)g^{d-1}/2$. Multiplying this by the typical largest favorable fluctuation in the number of facets (Eq. (6.13)) gives

$$U_{\text{gain}} \approx -\epsilon_g (1 - \epsilon) g^{d-1} f_L^{1/2} \left(\frac{L}{g}\right)^{(d-1)/2} \log^{1/2} \left(\frac{L}{g}\right). \tag{6.14}$$

To take advantage of this energy gain, the interface must make excursions from the cleavage plane of order the grain size. This leads to an energy cost of order

$$U_{\rm cost} \approx \epsilon_a \epsilon \ g L^{d-2}$$
.

Setting $U_{\rm gain} + U_{\rm cost} = 0$ we get

$$\frac{1-\epsilon}{\epsilon} = \frac{B\left(\frac{L}{g}\right)^{(d-3)/2}}{f_L^{1/2}\log^{1/2}\left(\frac{L}{g}\right)}.$$
 (6.15)

Where B is an undetermined constant that depends on the details of the grain structure, lattice structure, etc. In two dimensions Eq. (6.15) becomes

$$\frac{1-\epsilon}{\epsilon} = \frac{B}{f_L^{1/2} \left(\frac{L}{g}\right)^{1/2} \log^{1/2} \left(\frac{L}{g}\right)} \tag{6.16}$$

and in three dimensions

$$\frac{1-\epsilon}{\epsilon} = \frac{B}{f_L^{1/2} \log^{1/2} \left(\frac{L}{g}\right)}.$$
 (6.17)

From Eqns. (6.16) and (6.17) we can conclude that for large enough systems the cleavage

state is unstable to fluctuations for $any \epsilon < 1$ in both two and three dimensions. Often this is expressed as a critical length. In two dimensions, the logarithmic term is usually negligible. Omitting the logarithmic term in Eq. (6.16) we find that the critical length depends on grain size and grain boundary adhesion in the following way,

$$\frac{L_c}{g} = \frac{1}{f_L} \frac{(B\epsilon)^2}{(1-\epsilon)^2} = \frac{B^2 f(\epsilon)}{f_L}$$
(6.18)

where $f(\epsilon) = \epsilon^2/(1-\epsilon)^2$. In three dimensions, the logarithm is important and it leads to a critical length that is an exponential function of the grain boundary adhesion. From Eq. (6.17) we have

$$\frac{L_c}{g} = \exp\left(\frac{B^2 f(\epsilon)}{f_L}\right). \tag{6.19}$$

For sample sizes $L < L_c$ the lowest energy interfaces have constant roughness, while for sample sizes $L > L_c$ the interface roughens. L_c is also the linear size of the cleavage regions on the interface. These cleavage regions are terminated by steps which are of order the grain size. Thus the minimal energy surfaces are expected to be quite flat on length scales less than L_c and algebraically rough on larger length scales. The critical length decreases continuously with increasing ϵ . At the transition point to the weak adhesion limit (which occurs at $\epsilon \sim 1/2$) it becomes a constant and $L_c = g$. The formulae (6.18) and (6.19) are valid well above the transition to the weak adhesion limit.

In order to test the scaling theory, rewrite the roughness in terms of L_c

$$\frac{w}{g} = b_1 \left(\frac{L}{L_c}\right)^{\zeta}. \tag{6.20}$$

Using Eq. (6.20) and all of my data on a range of sample sizes and for a range of values of $\epsilon > 1/2$, I find the data of Fig. 6.9. The data follow the predictions of Eqns. (6.20) and (6.18) nicely, confirming the basic physics of roughening in these polycrystalline mi-

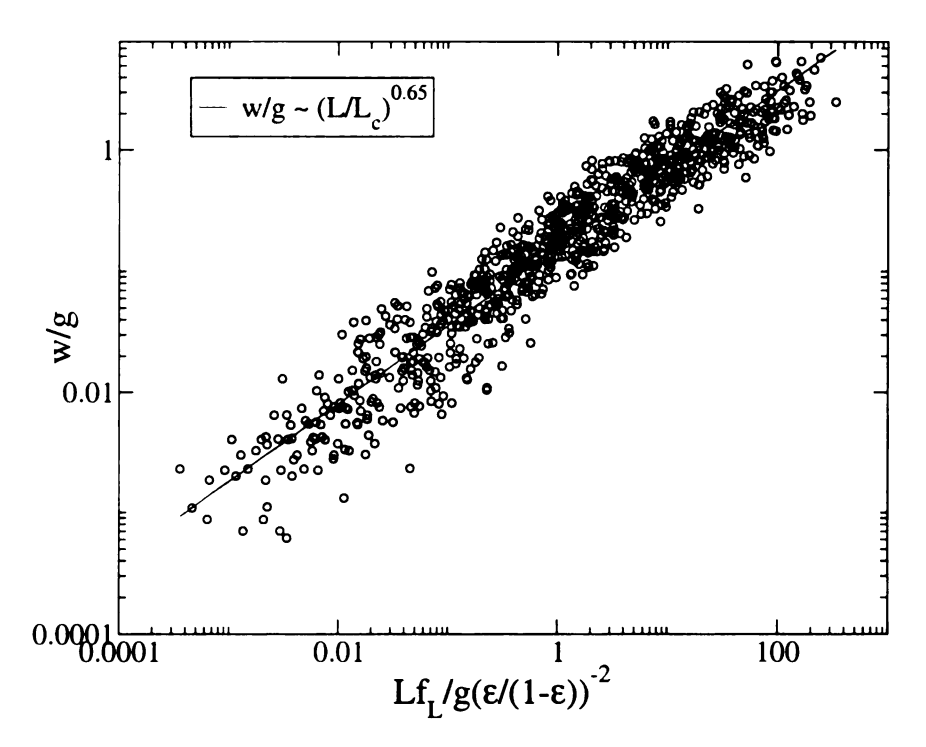


Figure 6.9: Scaling of roughness. The roughness w is plotted vs. L/L_c on a log-log scale. All data for $0.6 \le \epsilon \le 0.95$ and $w \ne 0$ is included. The roughness exponent $\zeta \simeq 2/3$.

crostructures.

From the theory developed above, it is straightforward to estimate the dependence on the adhesion energy of the roughness w, interface fraction f_i , energy E, and number of bonds N in the limit $\epsilon \to 1$.

Firstly, using Eqns. (6.18) and (6.20), the roughness as a function of ϵ behaves as

$$\frac{w}{L^{2/3}g^{1/3}} = B_1 \left(\frac{f_L}{f(\epsilon)}\right)^{\frac{2}{3}} \approx B_1 \delta \epsilon^{4/3} f_L^{2/3}$$
 (6.21)

where $\delta \epsilon = 1 - \epsilon$, and the last expression is the limiting behavior at small $\delta \epsilon$. The fraction

of minimum energy surface bonds which lie on grain boundaries is approximated by

$$f_i = \frac{g + (1 + \overline{h}) f_L L_c}{g + (1 + \overline{h}) f_L L_c + (1 - f_L) L_c}$$
(6.22)

$$= \frac{1 + (1 + \overline{h})B^2 f(\epsilon)}{1 + (\frac{1}{f_I} + \overline{h})B^2 f(\epsilon)}$$

$$(6.23)$$

$$\approx f_L \tag{6.24}$$

The total number of bonds on the minimal energy interface is approximated by

$$\begin{split} \frac{N}{L} &= \frac{g + (1 + \overline{h}) f_L L_c + (1 - f_L) L_c}{L_c} \\ &= 1 + \frac{g}{L_c} + \overline{h} f_L \\ &= 1 + \overline{h} f_L + \frac{f_L}{B^2 f(\epsilon)} \\ &\approx 1 + \overline{h} f_L + \frac{\delta \epsilon^2}{B^2} f_L \end{split}$$

Finally, the energy of the minimum energy surface is given by

$$\frac{E}{L\epsilon_g} = (1 - (1 - \epsilon)f_i) \frac{N}{L}$$

$$= \left(1 - (1 - \epsilon) \frac{1 + (1 + \overline{h})f(\epsilon)}{1 + (\frac{1}{f_L} + \overline{h})f(\epsilon)}\right)$$

$$\cdot \left(1 + \overline{h}f_L + \frac{f_L}{B^2f(\epsilon)}\right)$$

$$\approx (1 - (1 - \epsilon)f_L)(1 + \overline{h}f_L + \frac{\delta\epsilon^2}{B^2}f_L)$$

$$\approx 1 + \overline{h}f_L - \delta\epsilon f_L - \overline{h}\delta\epsilon f_L^2 + \frac{\delta\epsilon^2}{B^2}f_L - \frac{\delta\epsilon^3}{B^2}f_L^2.$$

For the grain structures I used, \overline{h} is not important. I therefore use the approximations

$$\frac{N}{L} \approx \frac{g + L_c}{L_c} = 1 + \frac{f_L}{B^2 f(\epsilon)} \tag{6.25}$$

and

$$\frac{E}{L\epsilon_q} \approx (1 - (1 - \epsilon)f_L) \left(1 + \frac{f_L}{Bf(\epsilon)} \right). \tag{6.26}$$

The fits using the data from $f_L \approx f_i$ are shown in Fig. 6.5 and Fig. 6.7.

The results of this section provide estimates of the behavior in the regime $1 > \epsilon > \epsilon_c$, where $\epsilon_c \sim 1/2$ for the grain structures used here in two dimensions.

6.5 Summary

There are three distinct fracture regimes. For $\epsilon < 1/2$ the minimum energy fracture surface follows the grain boundaries. For $1/2 < \epsilon < 1$ the interface includes both intragranular bonds and grain boundary bonds and is instable against roughening. For $\epsilon = 1$ the interface is a flat cleavage interface. In the weak adhesion regime the minimal energy surfaces follow the grain boundaries and are described by scaling theories that have been developed for the roughness of domain walls in Ising magnets, but with a renormalized length scale L/g. The ideal cleavage state at $\epsilon = 1$ is unstable to fluctuations, so that any small reduction of the grain boundary bonding from $\epsilon = 1$ leads to a mixed interface mode on long length scales.

We have developed a scaling theory to describe the behavior of the energy and interface morphology in the mixed interface phase. In the mixed phase, in both two and three dimensions, the minimum energy interface is flat on length scales $L < L_c$ but it is rough on length scales $L \gg L_c$. The dependence of L_c on the grain size and the grain boundary adhesion is a power law in two dimensions (see Eq. (6.18)), while this dependence is exponential in three dimensions (see Eq. (6.19)). The scaling laws in two dimensions are confirmed by large scale simulations (see Fig. 6.9).

Chapter 7

Outlook

In both physics and computer science disordered systems serve as models for complexity. Each discipline has developed methods for the study of disordered systems. Computer Science studies are traditionally case studies concentrating on instances rather than averages. Statistical physics, on the other hand, deals with the average properties and fluctuations of ensembles. Erdös' study of randomly diluted graphs, for example, complements percolation and is really a study of phase transitions. The methods of the study of phase transitions allow a better classification of NP-hard problems.

Although the random-field Ising Model has been studied for over three decades there are still many fundamental questions open. The magnetization exponent β for the RFIM in 3D is approximately 0. Neither numerical analysis nor experiment will be able to distinguish between a first and second order phase transition based on the magnetization. A better way to decide the order of the transition might be to analyze the percolation behavior of the majority and minority spin clusters. Other open question are: why does the infinite-range model fail to predict a phase transition for certain distributions of random fields, and why do the results obtained on the Cayley tree differ from those of the infinite-range model even in the $z \to \infty$ limit?

My numerical analysis of the interface roughness in Chapter 6 is limited to 2D. The natural next step is to do the numerics in 3D and test the scaling prediction. In 3D other mechanisms, e.g., partial facet fracture, may play a role. In addition to the scaling of minimal surfaces the scaling of shortest paths in polycrystalline materials is important. Further improvements to the model should include an angle dependent adhesion energy.

Appendix A

Taylor Expansion of P_+ for the RFIM on the Cayley Tree

I want to show that the second order term in the Taylor expansion of the steady state solution of P_+ disappears for general α .

The steady state equation for the RFIM on the Cayley tree is

$$x = \sum_{g=0}^{\alpha} \begin{pmatrix} \alpha \\ g \end{pmatrix} x^g (1-x)^{\alpha-g} a_+(\alpha, g)$$

Expand this in a Taylor series around x = 1/2.

$$f(x) = f(0) + f'(0)x + \frac{1}{2}f''(0)x^2 + \cdots$$

The zeroth order term in the series is

The first order term, f'(0), is

$$\begin{split} f'(0) &= \left. \frac{\partial}{\partial x} \sum_{g=0}^{\alpha} \left(\begin{array}{c} \alpha \\ g \end{array} \right) \left(\frac{1}{2} + x \right)^g \left(\frac{1}{2} - x \right)^{\alpha - g} a_+(\alpha, g) \right|_{x=0} \\ &= \left. \sum_{g=0}^{\alpha} \left(\begin{array}{c} \alpha \\ g \end{array} \right) a_+(\alpha, g) \left[g \left(\frac{1}{2} + x \right)^{g-1} \left(\frac{1}{2} - x \right)^{\alpha - g} \\ &- (\alpha - g) \left(\frac{1}{2} + x \right)^g \left(\frac{1}{2} - x \right)^{\alpha - g-1} \right] \right|_{x=0} \\ &= \left. \sum_{g=0}^{\alpha} \left(\begin{array}{c} \alpha \\ g \end{array} \right) a_+(\alpha, g) \left[g \left(\frac{1}{2} \right)^{g-1} \left(\frac{1}{2} \right)^{\alpha - g} - (\alpha - g) \left(\frac{1}{2} \right)^g \left(\frac{1}{2} \right)^{\alpha - g-1} \right] \right] \\ &= \left. \frac{1}{2^{(\alpha - 1)}} \sum_{g=0}^{\alpha} \left(\begin{array}{c} \alpha \\ g \end{array} \right) a_+(\alpha, g) (2g - \alpha) \\ &= \frac{1}{2^{(\alpha - 1)}} \left(\begin{array}{c} \alpha \\ 0 \end{array} \right) a_+(\alpha, 0) (-\alpha) + \left(\begin{array}{c} \alpha \\ 1 \end{array} \right) a_+(\alpha, 1) (2 - \alpha) + \cdots \\ &+ \left(\begin{array}{c} \alpha \\ \alpha - 1 \end{array} \right) a_+(\alpha, \alpha) (\alpha - 2) + \left(\begin{array}{c} \alpha \\ \alpha \end{array} \right) a_+(\alpha, \alpha) \alpha \\ &= \frac{1}{2^{(\alpha - 1)}} \sum_{g=0}^{\alpha/2} \left(\begin{array}{c} \alpha \\ g \end{array} \right) (2g - \alpha) (1 - 2a_+(\alpha, g)) \end{split}$$

The second order term is

$$\begin{split} f''(0) &= \frac{\partial}{\partial x} f'(x) \\ &= \sum_{g=0}^{\alpha} \begin{pmatrix} \alpha \\ g \end{pmatrix} a_{+}(\alpha, g) \left[g(g-1) \left(\frac{1}{2} + x \right)^{g-2} \left(\frac{1}{2} - x \right)^{\alpha - g} \right. \\ &- g(\alpha - g) \left(\frac{1}{2} + x \right)^{g-1} \left(\frac{1}{2} - x \right)^{\alpha - g-1} + \\ &+ (\alpha - g)(\alpha - g - 1) \left(\frac{1}{2} + x \right)^{g} \left(\frac{1}{2} - x \right)^{\alpha - g-2} \\ &- g(\alpha - g) \left(\frac{1}{2} + x \right)^{g-1} \left(\frac{1}{2} - x \right)^{\alpha - g-1} \right] \bigg|_{x=0} \\ &= \frac{1}{2^{\alpha - 2}} \sum_{g=0}^{\alpha} \begin{pmatrix} \alpha \\ g \end{pmatrix} a_{+}(\alpha, g) \left[g(g-1) - g(\alpha - g) + (\alpha - g)(\alpha - g - 1) - g(\alpha - g) \right] \\ &= \frac{1}{2^{\alpha - 2}} \sum_{g=0}^{\alpha} \begin{pmatrix} \alpha \\ g \end{pmatrix} a_{+}(\alpha, g) \left[g^{2} - g - \alpha g + g^{2} + \alpha^{2} - \alpha g - \alpha - \alpha g + g^{2} + g \right. \\ &- \alpha g + g^{2} \right] \\ &= \frac{1}{2^{\alpha - 2}} \sum_{g=0}^{\alpha} \begin{pmatrix} \alpha \\ g \end{pmatrix} a_{+}(\alpha, g) \left[4g^{2} - 4\alpha g + \alpha^{2} - \alpha \right] \\ &= \frac{1}{2^{\alpha - 2}} \sum_{g=0}^{\alpha} \begin{pmatrix} \alpha \\ g \end{pmatrix} a_{+}(\alpha, g) \left[(2g - \alpha)^{2} - \alpha \right] \\ &= -\frac{\alpha}{2^{\alpha - 2}} \sum_{g=0}^{\alpha} \begin{pmatrix} \alpha \\ g \end{pmatrix} a_{+}(\alpha, g) + \frac{1}{2^{\alpha - 2}} \sum_{g=0}^{\alpha} \begin{pmatrix} \alpha \\ g \end{pmatrix} a_{+}(\alpha, g)(2g - \alpha)^{2} \\ &= -2\alpha + \frac{1}{2^{\alpha - 2}} \sum_{g=0}^{\alpha/2} \begin{pmatrix} \alpha \\ g \end{pmatrix} a_{+}(\alpha, g)(2g - \alpha)^{2} \\ &= 0 \end{split}$$

Where the sum up to $\alpha/2$ for α odd means the sum up to $(\alpha-1)/2$. For even α $a_+(\alpha,\alpha/2)=1/2$ does not disappear from the sum. It contributes 1/2 $\begin{pmatrix} \alpha \\ \alpha/2 \end{pmatrix}$ to the total sum, which gives $\sum_{g=0}^{\alpha/2} \begin{pmatrix} \alpha \\ g \end{pmatrix} = 2^{\alpha-1}$.

Bibliography

- [1] Amnon Aharony. Tricritical points in systems with random fields. *Phys. Rev. B*, 18(7):3318–3327, October 1978. Mean field approach and renormalization group theory applied to the RFIM.
- [2] M. J. Alava and P. M. Duxbury. Disorder-induced roughening in the three-dimensional ising model. *Physical Review B*, 54(21):14990–14993, December 1996.
- [3] M. J. Alava, P. M. Duxbury, C. F. Moukarzel, and H. Rieger. *Exact Combinatorial Algorithms: Ground States of Disordered Systems*, volume 18 of *Phase Transitions and Critical Phenomena*. Academic Press, 2001.
- [4] Réka Albert and Albert-László Barabássi. Statistical mechanics of complex networks. arXiv:cond-mat/0106096, 6 June 2001.
- [5] M. P. Anderson, D. J. Srolovitz, G.S. Grest, and P.S. Shani. Computer simulation of grain growth .1. kinetics. *Acta Metallurgica*, 32:783–791, 1984.
- [6] George B. Arfken and Hans J. Weber. *Mathematical Methods for Physicists*. Academic Press, 4th edition, 1995.
- [7] P. D. Beale and D. J. Srolovitz. Elastic fracture in random materials. *Physical Review* B, 37(10):5500 5507, APR 1 1988.
- [8] E. Bouchaud. Scaling properties of cracks. *Journal of Physics-Condensed Matter*, 9(21):4319 4344, MAY 26 1997.
- [9] J. P. Bouchaud and A. Georges. Competition between lattice pinning and impurity pinning variational theory and physical realizations. *Physical Review Letters*, 68(26):3908 3911, JUN 29 1992.
- [10] R. Bruinsma. Random-field Ising model on a Bethe lattice. *Physical Review B*, 30(1):289–299, July 1984.
- [11] B. V. Cherkassky and A. V. Goldberg. On implementing the push-relabel method for the maximum flow problem. *Algorithmica*, 19(4):390–410, Dec 1997.
- [12] Clay Mathematics Institute. The P versus NP problem. Clay Mathematics Institute.

- [13] J.-C. Anglès D'Auriac and N. Sourlas. The 3d random field ising model at zero temperature. *Europhys. Lett.*, 39(5):473-478, 1997.
- [14] Deepak Dhar, Prabodh Shukla, and James P. Sethna. Zero-temperature hysteresis in the random-field Ising model on a Bethe lattice. *J. Phys. A: Math Gen.*, 30:5259–5267, 1997.
- [15] T. Emig and T. Nattermann. Disorder driven roughening transitions of elastic manifolds and periodic elastic media. *European Physical Journal B*, 8(4):525 546, APR 1999.
- [16] P. Erdös and A. Rènyi. On random graphs I. Publ. Math. Debrecen, 6:290–297, 1959.
- [17] Daniel S. Fisher. Interface fluctuations in disordered systems: 5- epsilon expansion and failure of dimensional reduction. *Physical Review Letters*, 56:1964, 1986.
- [18] Shmuel Fishman and Amnon Aharony. Random field effects in disordered anisotropic antiferromagnets. J. of Phys. C: Solid State Phys., 12:L729–L733, 1979.
- [19] A.V. Goldberg and R.E. Tarjan. A new approach to the maximum-flow problem. Journal of the Association for Computing Machinery, 35(4):921–940, October 1988.
- [20] Alexander K. Hartmann and U. Nowak. Universality in three-dimensional random field ground states. *cond-mat/9807131*, 1998.
- [21] Alexander K. Hartmann and Martin Weigt. Statistical mechanics perspective on the phase transition in vertex covering of finite-connectivity random graphs. *cond-mat/0006316*, June 2000.
- [22] Gregory N. Hassold and Elizabeth A. Holm. A fast serial algorithm for the finite temperature quenched Potts model. *Computers in Physics*, 7(1):97–107, 1993.
- [23] E. A. Holm. Surface formation energy for intergranular fracture in two-dimensional polycrystals. *Journal of the American Ceramic Society*, 81(3):455 459, MAR 1998.
- [24] Elizabeth A. Holm and Corbette C. Battaile. The computer simulation of microstructural evolution. *Journal of The Minerals, Metals & Materials Society*, 53(9):20–23, 2001.
- [25] Kerson Huang. Statistical mechanics. John Wiley & Sons, Inc, 2 edition, 1987.
- [26] David A. Huse and Christopher L. Henley. Pinning and roughening of domain walls in Ising systems due to random impurities. *Physical Review E*, 54:2708, 1985.
- [27] John Z. Imbrie. Lower critical dimension of the random-field Ising model. *Physical Review Letters*, 53(18):1747–1750, 29 August 1984.

- [28] Yoseph Imry and Shang keng Ma. Random-field instability of the ordered state of continuous symmetry. *Physical Review Letters*, 35(21):1399–1401, 1975.
- [29] Ernst Ising. Beitrag zur Theorie des Ferro- und Paramagnetismus. PhD thesis, Universität Hamburg, 1924.
- [30] Ernst Ising. Beitrag zur Theorie des Ferromagnetismus. Zeitschrift für Physik, 31:253–258, 1925.
- [31] Svante Janson, Tomasz Łuczak, and Andrzej Rucinski. *Random Graph*. John Wiley & Sons, Inc., 2000.
- [32] Dieter Jungnickel. *Graphen, Netzwerke und Algorithmen*. BI Wissenschaftsverlag, 3 edition, 1994.
- [33] Mark Kac. Statistical Physics, phase transitions, and superfluidity, volume 1, chapter Mathematical mechanisms of phase transitions, page 241. Gordon and Breach, New York, 1968.
- [34] L. P. Kadanoff. *Physics*, 2:263, 1966.
- [35] Sigismund Kobe. Ernst Ising Physicist and teacher. *Journal of Statistical Physics*, 88(3-4):991–995, August 1997.
- [36] Wilhelm Lenz. Phys. ZS., 21:613, 1920.
- [37] Kurt Mehlhorn, Stefan Naeher, et al. LEDA, the Library of Efficient Data types and Algorithms. LEDA is now published by Algorithmic Solutions and is available at www.algorithmic-solutions.com.
- [38] A. Alan Middleton. Numerical results for the ground-state interface in a random medium. *Physical Review E*, 52:R3337–R3340, October 1995.
- [39] Andrew T. Ogielski. Integer optimization and zero-temperature fixed point in Ising random-field systems. *Physical Review Letters*, 57(10):1251–1254, September 1986. First paper using maxflow to determine magnetization in groundstate.
- [40] R Peierls. On Ising's model of ferromagnetism. P. Cambridge Philos. S., 32:477, 1936.
- [41] V. I. Raisanen, E. T. Seppälä, M. J. Alava, and P. M. Duxbury. Quasistatic cracks and minimal energy surfaces. *Physical Review Letters*, 80(2):329 332, JAN 12 1998.
- [42] L. E. Reichl. A Modern Course in Statistical Physics. University of Texas Press, 1980.
- [43] Steffen Reith and Heribert Vollmer. Wer wird Millionär? Komplexitätstheorie: Konzepte und Herausforderungen. c't, (07):240–251, 2001.

- [44] M. Sahimi and J. D. Goddard. Elastic percolation models for cohesive mechanical failure in seterogeneous systems. *Physical Review B*, 33(11):7848 7851, JUN 1 1986.
- [45] E. T. Seppälä, M. J. Alava, and P. M. Duxbury. Intermittence and roughening of periodic elastic media art. no. 036126. *Physical Review E*, 6303(3):6126 +, MAR 2001.
- [46] Nicolas Sourlas. Universality in random systems: The case of the 3-d random-field Ising model. *unpublished*, 1998.
- [47] D. J. Srolovitz, M. P. Anderson, P. S. Sahni, and G. S. Grest. Computer simulation of grain growth .2. grain-size distribution, topology and local dynamics. *Acta Metallurgica*, 32:793–802, 1984.
- [48] H. Eugene Stanley. *Introduction to Phase Transitions and Critical Phenomena*. Oxford University Press, 1971.
- [49] Dietrich Stauffer and Amnon Aharony. *Introduction to Percolation Theory*. Taylor & Francis, revised 2nd edition, 1994.
- [50] A.P. Sutton and R.W. Baluffi. *Interfaces in Crystalline Materials*. Oxford University Press, 1995.
- [51] Michael R. Swift, A. J. Bray, Amos Maritan, Marek Cieplak, and Jayanth R. Banavar. Scaling of the random-field Ising model at zero temperature. *Europhys. Lett.*, 38(4):273–278, 1 May 1997.
- [52] Michael R. Swift, Amos Maritan, Marek Cieplak, and Jayanth R. Banavar. Phase diagrams of random-field Ising systems. *Journal of Physics A: Math. Gen.*, 27:1525–1532, 1994.
- [53] D. I. Uzunov. *Introduction to the Theory of Critical Phenomena*. World Scientific, 1993.
- [54] J. D. Verhoeven, A. H. Pendray, and W. E. Dauksch. The key role of impurities in ancient Damascus steel blades. *Journal of The Minerals, Metals & Materials Society*, 50(9):58-64, 1998.
- [55] John D. Verhoeven. The mystery of Damascus blades. *Scientific American*, 284(1):74–79, January 2001.
- [56] Martin Weigt and Alexander K. Hartmann. Number of guards needed by a museum: A phase transition in vertex covering of random graphs. *Physical Review Letters*, 84(26):6118–6121, June 2000.

- [57] Martin Weigt and Alexander K. Hartmann. Minimal vertex covers on finite-connectivity random graphs a hard-sphere lattice picture. *Physical Review E*, 63:056127, 2001.
- [58] Martin Weigt and Alexander K. Hartmann. Typical solution time for a vertex-covering algorithm on finite-connectivity random graphs. *Physical Review Letters*, 86(8):1658–1661, February 2001.
- [59] A. Zangwill. Physics at Surfaces. Cambridge University Press, 1988.

Glossary

- Manifold A topological space that is locally flat, or Euclidian. More formally, for every point in a manifold there exists a neighborhood and a continuous transformation of that neighborhood into an open unit ball of the same dimension.
- **NP** Nondeterministic Polynomial. A class of problems in computer science where a known solution can be verified in polynomial time.
- **NP-complete** A class of problems in computer science that has no known polynomial algorithm for all problem instances but a solution can be verified in polynomial time. Each problem of the class can be mapped into any other NP complete problem by a polynomial algorithm.

Index

Cayley tree, 25–26	quenched disorder, 32
percolation, 35–38 RFIM, 66–69 complete graph, 38 critical exponent, 11 cut, 45	random graph, 38 random-bond Ising model, 41 random-field Ising model, 42 RBIM, see random-bond Ising model renormalization group, 28 residual graph, 50 RFIM, see random-field Ising model Rushbrooke equality, 16
edges, 38 flow feasible, 45	
giant cluster, 38	scaling hypothesis, 12
graph, 38	traveling salesman, 2
homogeneous functions, 13 hyperscaling, 17	universality class, 29
Josephson law, 17	vertex cover, 2
Landau theory, 29–32 lattice gas, 3	Widom equality, 16 Zustandsfunktion, 12
manifold, 40, 109 maximal independent set, 3 maximum flow algorithm augmenting path, 50 push relabel, 52 maximum flow/minimum cut theorem, 45	
nodes, 38 nondeterministic polynomial, 2, 109 NP, see nondeterministic polynomial NP-complete, 3, 109	
partition function, 12 percolation, 32–39 bond percolation, 32 site percolation, 33	

